Research Report
Agreement T2695 Task 61
Single Loop Video Data

IMPROVING TRUCK AND SPEED DATA USING PAIRED VIDEO AND SINGLE-LOOP SENSORS

by

Yinhai Wang
Assistant Professor

Nancy L. Nihan
Professor/Director
Transportation Northwest

Ryan P. Avery
Graduate Research Assistant

Guohui Zhang
Graduate Research Assistant

Department of Civil and Environmental Engineering
University of Washington
Seattle, Washington 98195-2700

Washington State Transportation Center (TRAC)
University of Washington, Box 354802
1107 NE 45th Street, Suite 535
Seattle, Washington 98105-4631

Washington State Department of Transportation Technical Monitor
Ted Trepanier, State Traffic Engineer

Sponsored by

Washington State Transportation Commission
Washington State Department of Transportation
Olympia, Washington 98504-7370

Transportation Northwest (TransNow)
University of Washington
135 More Hall, Box 352700
Seattle, Washington 98195-2700

and in cooperation with
U.S. Department of Transportation
Federal Highway Administration

December 2006

TECHNICAL REPORT STANDARD TITLE PAGE

WA-RD 656.1	2. GOVERNMENT ACCESSION NO.	3. RECIPIENT'S CATALOG NO.
4. TITLE AND SUBTITLE Improving Truck and Speed Data Using Paired Video and Single-Loop Sensors		5. REPORT DATE December 2006 6. PERFORMING ORGANIZATION CODE
7. AUTHOR(S) Yinhai Wang, Nancy Nihan, Ryan Avery, and Guohui Zhang		8. PERFORMING ORGANIZATION REPORT NO. TNW
9. PERFORMING ORGANIZATION NAME AND ADDRESS Washington State Transportation Center (TRAC) University of Washington, Box 354802 University District Building; 1107 NE 45th Street, Suite 535 Seattle, Washington 98105-4631		10. WORK UNIT NO. 11. CONTRACT GRANT NO. Agreement T2695 Task 61
12. SPONSORING AGENCY NAME AND ADDRESS Research Office Washington State Department of Transportation Transportation Building, MS 47372 Olympia, Washington 98504-7372 14 Doug Brodin, Project Manager, 360-705-7972		13. TYPE OF REPORT AND PERIOD COVERED Final Research Report 14. SPONSORING AGENCY CODE

15. SUPPLEMENTARY NOTES

This study was conducted in cooperation with the University of Washington and the US Department of Transportation

16. ABSTRACT

Real-time speed and truck data are important inputs for modern freeway traffic control and management systems. However, these data are not directly measurable by single-loop detectors. Although dual-loop detectors provide speeds and classified vehicle volumes, there are too few of them on our current freeway systems to meet the practical needs of advanced traffic management systems. This makes it extremely desirable to develop appropriate algorithms to calculate speed and truck volume from single-loop outputs or from video data.

To obtain quality estimates of traffic speed and truck volume data, several algorithms were developed and implemented in this study. These algorithms are (1) a speed estimation algorithm based on the region growing mechanism and single-loop measurements; (2) a set of computer – vision-based algorithms for extracting background images from a video sequence, detecting the presence of vehicles, identifying and removing shadows, and calculating pixel-based vehicle lengths for classification; and (3) a speed estimation algorithm that uses paired video and single-loop sensor inputs. These algorithms were implemented in three distinct computer applications. Field-collected video and loop detector data were used to test the algorithms.

Our test results indicated that quality speed and truck volume data can be estimated with the proposed algorithms by using single-loop data, video data, or both video and single-loop data. The Video-based Vehicle Detection and Classification (VVDC) system, based on the proposed video image processing algorithms, provides a cost-effective solution for automatic traffic data collection with surveillance video cameras. For locations with both video and single-loop sensors, speed estimates can be improved by combining video data with single-loop data.

17. KEY WORDS Trucks, Data Collection, Computer Vision, Loop Detectors, Vehicle Classification, Video Image Processing, Speed		18. DISTRIBUTION STATEMENT	
19. SECURITY CLASSIF. (OF THIS REPORT) None	20. SECURITY CLASSIF. (OF THIS PAGE) None	21. NO. OF PAGES	22. PRICE

DISCLAIMER

The contents of this report reflect the views of the authors, who are responsible for the facts and accuracy of the data presented herein. This document is disseminated through the Transportation Northwest (TransNow) Regional Center under the sponsorship of the U.S. Department of Transportation UTC Grant Program and through the Washington State Department of Transportation. The U.S. Government assumes no liability for the contents or use thereof. Sponsorship for the local match portion of this research project was provided by the Washington State Department of Transportation. The contents do not necessarily reflect the views or policies of the U.S. Department of Transportation or Washington State Department of Transportation. This report does not constitute a standard, specification, or regulation.

TABLE OF CONTENTS

LIST OF FIGURES

LIST OF TABLES

EXECUTIVE SUMMARY

Traffic speed and truck volume data are important variables for transportation planning, pavement design, traffic safety, traffic operations, and car emission controls. However, these data are not directly measured by single-loop detectors, which are the most widely available type of sensor on roadway networks in the U.S. In order to obtain quality estimates of traffic speed and truck volume data from single-loop detectors and from video detectors, several algorithms were developed and tested in this study.

First, a new speed estimation algorithm that uses single-loop data was developed. This algorithm applies the region growing mechanism commonly used in video image processing. This region growing algorithm, together with a vehicle classification algorithm based on the Nearest Neighbor Decision (NND) rule, was implemented in the single-loop Speed and Truck volume Estimator (ST-Estimator) for improved speed and truck volume data. Test results on the ST-Estimator indicated that the new speed algorithm achieved much better accuracy than the traditional algorithm used by most traffic management centers. By using the speed estimated with the new algorithm, long vehicle (LV) volumes can be estimated for vehicle classification purposes on the basis of the NND rule. LV volume errors estimated at three test locations in Seattle (the second lanes at station ES-167D, station ES-172R, and station ES-209D) were within 7.5 percent over a 24-hour period. The ST-Estimator test results indicated that the ST-Estimator can be employed to obtain reasonably accurate speed and LV volume estimates at single-loop stations.

Second, several computer –vision-based algorithms were developed or applied to extract the background image from a video sequence, detect the presence of vehicles,

identify and remove shadows, and calculate pixel-based vehicle lengths for classification. These algorithms were implemented in the prototype Video-based Vehicle Detection and Classification (VVDC) system by using Microsoft Visual C#. As a plug and play system, the VVDC system is capable of processing live video signals in real time. The VVDC system can also be used to process digitized video images in the JPEG or BMP formats. Because the VVDC system does not require camera calibration, it can be easily applied to locations with surveillance video cameras. Also, users are allowed to specify the bin threshold to collect desired types of vehicles. The VVDC system was tested at three test locations under different traffic and environmental conditions. The accuracy for vehicle detection was above 97 percent, and the total truck count error was lower than 9 percent for all three tests. This suggests that the video image processing method developed for vehicle detection and classification in this study is indeed a viable alternative for truck data collection. However, the prototype VVDC system is currently designed to work in the daytime and under conditions without longitudinal vehicle occlusion and severe camera vibration.

Third, a speed estimation algorithm that uses paired video and single-loop sensor inputs was designed. The core idea of this algorithm was to use a video sensor to screen out intervals with LVs before single-loop measurements were applied to the traditional algorithm for speed estimation. Because the presence of LVs violates the uniform vehicle length assumption for the traditional algorithm of speed estimation, intervals containing LVs must be properly addressed to avoid speed estimation bias. The paired video and single-loop sensors rely on video image processing for LV detection and single-loop data for speed calculation. If an interval is identified to contain one or more

LVs, its single-loop measurements are dropped from the speed estimation. Instead, the most recently calculated interval speed is assigned to this interval. The paired video and single-loop algorithm was implemented in the Paired VL system. Evaluation of the Paired VL system showed that speeds estimated by this system were more accurate than speeds estimated with the traditional algorithm. However, finding a location with both video and single-loop sensors may not be easy. Also, time synchronization for the Paired VL system is very challenging and detection errors from the video sensor may significantly degrade the performance of the Paired VL system. All these factors cast doubt over the applicability of the Paired VL system, although the effectiveness of the idea was demonstrated in this study.

In summary, several algorithms and corresponding computer tools for improved speed and truck data were developed during this study. The authors conclude that quality speed and truck volume data can be estimated from single-loop data by applying the ST-Estimator. Although the prototype VVDC system works only under relatively ideal conditions, the utility and effectiveness of the system were demonstrated in this study. Given that surveillance video cameras have been increasingly deployed in recent years, the VVDC system can be a cost-effective solution for turning these surveillance video cameras into video detectors when necessary. For locations with both video and single-loop sensors, speed estimates can be improved by combining video data with single-loop data.

PART I RESEARCH BACKGROUND

1.0 INTRODUCTION

1.1 RESEARCH BACKGROUND

Traffic speed is one of the most important variables for traffic operations and control. It is both a potential sign of problems on the roadway and a good measure of system effectiveness. Many incident detection algorithms are based on traffic speed data. Speed variation is also a good indicator of traffic safety (Anderson and Krammes, 2000). If good network-wide speed information is available, the travel time for any origin-destination pair can be calculated.

Data concerning trucks and heavy vehicles are important for several reasons. Because of their heavy weight and large turning radii, long vehicles (LVs) have very different moving characteristics than short vehicles (SVs), which are mostly passenger cars. This affects a roadway's geometric design factors, such as horizontal alignment and curb heights. The heavy weight of such vehicles is also an important factor in pavement design and maintenance, as truck volumes influence both pavement life and design parameters (AASHTO, 2004). Roadway performance is influenced by the presence of large and/or low-performance vehicles in the traffic stream because they reduce roadway capacity (Cunagin and Messer, 1983). The Highway Capacity Manual (TRB, 2000) explicitly stipulates that passenger-car equivalents of LVs under different conditions should be used for highway design. Safety is also influenced by LVs. A recent study found that 8 percent of fatal vehicle-to-vehicle crashes involved large trucks, although only 3 percent of all registered vehicles were large trucks (NHTSA, 2004). Recent studies (Peters et al., 2004; Kim et al., 2004) also found that particulate matter (PM) is

strongly associated with the onset of myocardial infarction and respiratory symptoms. Heavy duty trucks that use diesel engines are major sources of PM, accounting for 72 percent of traffic-emitted PM (EPA, 2001).

All these facts illustrate that good speed and truck volume data are extremely important for accurate analysis of traffic safety, traffic pollution, and flow characteristics in transportation planning, management, and engineering. They are also important inputs for advanced traffic management systems (ATMS) and advanced traveler information systems (ATIS). Additionally, truck volume data are needed by federal and state transportation organizations to adequately monitor and analyze our nation's freight movements.

The Washington State Department of Transportation's (WSDOT's) dual-loop detection system classifies vehicles into four bins according to their lengths. The four length categories are described in Table 1-1. Because of variations in the lengths of vehicles within specific FHWA vehicle classes, the four WSDOT length classes do not directly relate to the 13 FHWA vehicle classes (Hallenbeck, 1993). Typically, vehicles 40 ft and longer are referred to as LVs (Wang and Nihan, 2003; Kwon et al., 2003), and those shorter than 40 ft are referred to as short vehicles (SVs). The majority of LVs on Seattle area freeways are trucks. Hence LVs and trucks are used interchangeably in this report.

Table 1-1: WSDOT Dual-loop Length Classification

Class	Length Range (feet)	Vehicle types
Bin 1	Less than 26	Cars, pickups, and short single-unit trucks
Bin 2	From 26 to 39	Cars and trucks pulling trailers, long single-unit trucks
Bin 3	From 40 to 65	Combination trucks
Bin 4	Longer than 65	Multi-trailer trucks

1.2 PROBLEM STATEMENT

Since its introduction in the early 1960s, the inductance loop detector has become the most popular form of vehicle detection system (ITE, 1997). Many freeway corridors contain single-loop detectors for collecting volume (the number of vehicles passing per unit time) and lane occupancy (the fraction of some total time interval that a loop is occupied by vehicles) data. These data are valuable sources for transportation planning and traffic operations. However, recent developments in ATMS require increasingly more accurate and timely speed and vehicle-classification data, which are not directly measurable by single-loop detectors. To obtain such speed and vehicle-classification data, dual-loop detectors are typically employed.

A dual-loop detector is formed by two consecutive single-loop detectors separated by several meters. It is also called a speed trap or double-loop detector. Because a dual-loop detector is capable of recording the time for a vehicle to traverse from the first loop to the second loop, and the distance between the two loops is predetermined, a dual-loop detector can calculate the speed of a vehicle fairly accurately. By applying the calculated speed and single-loop measured lane occupancies, the length of a vehicle can also be estimated, and the vehicle can be assigned to a certain class on the basis of its length. However, although dual-loop detectors are ideal for collecting speed and vehicle-

classification data, there are too few of them on our current freeway systems to meet practical ATMS and ATIS needs, and the cost of upgrading a single-loop detector to a dual-loop detector is high. According to the experience of the WSDOT, the cost for upgrading from a single-loop detector to a dual-loop detector ranges from $3250 to $5750 (includes $750 direct cost for loop placement and $2500 - $5000 indirect cost caused by lane closure) (Wang and Nihan, 2003). In addition, most dual-loop detectors deployed in the greater Seattle area are reported to have serious under-count or over-count problems for bin volumes (Zhang et al., 2003). Therefore, making existing single-loop detectors capable of providing better speed and vehicle-classification data is of practical significance for traffic researchers.

To meet ATMS and ATIS needs, new sensors that are capable of collecting speed and truck volume data have been developed in recent years. Among these new sensors, video image processors (VIPs) are noteworthy. These systems offer the advantage of preserving a continuous stream of information rather than recording discrete vehicle passages, as in most other detection systems. Examples of such programs include the Vantage Express system developed by Iteris, Inc. and the VideoTrack system developed by Peek Traffic Inc. These systems can operate during both daytime and nighttime conditions. Some of these systems claim to be capable of detecting vehicles in unfavorable weather conditions. However, the cost for such systems is significant, and they require calibrated camera images to work correctly. Calibrating these systems normally requires very specific road surface information (such as the distance between recognizable road surface marks) and/or camera information (such as the elevation and tilt angle), which may not be easy to obtain (Avery et al., 2004). Furthermore, recent

studies (Bonneson and Abbas, 2002; Martin et al., 2004; Rhodes et al, 2005) that evaluated some of these commercial systems found that shadows and headlight reflections generated significant false detection problems (a false detection occurs when a "no" event is recorded as a "yes") and early detections. These commercial systems typically require concurrent installation of proprietary hardware and software, especially for intersection video traffic detection. Proprietary equipment prevents agencies from modifying or improving the algorithms used in traffic detection to better suit their needs. Although some vendors do allow for flexibility in hardware selection, the software remains immutable in its treatment of traffic detection and underlying assumptions.

The aforementioned commercial systems are not the only ones that require calibration. According to Tian et al. (2002), all the available video-image systems require calibration of field of view based on field measurements of certain geometric roadway elements before the data collection process can be initiated. This calibration requirement leads to problematical system inflexibility – if the camera position is changed, the calibration measurements may need to be retaken. Therefore, cameras that provide input to VIPs are normally fixed.

In the greater Seattle area, over 250 surveillance video cameras have been installed along major freeways. These video cameras are typically used by traffic operators, who can pan, tilt, and zoom the camera view to monitor traffic conditions. To accommodate the need for various screen views, these cameras are generally not calibrated. For many locations, road surface marks are not at all available for calibrating these cameras. Consequently, none of these surveillance video cameras have been used for automatic data collection with VIPs.

1.3 RESEARCH OBJECTIVE

Considering that single-loop detectors are still the major source of live traffic data and that surveillance video cameras have been widely deployed along urban freeways, this research aimed to improve truck and speed data by using existing single-loop sensors and surveillance video cameras. Specifically, we had the following three objectives:

- design and implement a new algorithm that uses single-loop measurements for speed and truck data estimation
- develop a prototype plug and play Video-based Vehicle Detection and Classification (VVDC) system for truck data collection that would use un-calibrated video images
- explore the feasibility of pairing video and single-loop sensors for better speed estimates. Develop and test a computer application that combines single-loop measurements and vehicle length calculated by the VVDC system for improved speed calculation.

2.0 STATE OF THE ART

2.1 ESTIMATING SPEED AND TRUCK VOLUMES USING SINGLE-LOOP MEASUREMENTS

As mentioned earlier, a single-loop detector merely measures volume and lane occupancy. Algorithms have been proposed to estimate traffic speed and truck volumes with single-loop measurements. One of the earliest investigations into estimating speed from single-loop outputs began with the landmark speed estimation formula proposed by Athol (1965), which was further examined by Mikhalkin et al. (1972), Gerlough and Huber (1975), and Courage et al (1976) and has been the principal equation for many subsequent works:

$$\overline{s}_s(i) = \frac{V(i)}{T \cdot O(i) \cdot g} \tag{2-1}$$

where i = time interval index;
$\overline{s}_s$ = space mean speed in mph for each interval
V = vehicles per interval
O = lane occupancy in percentage of time the detector is occupied
T = the number of hours per interval
g = speed estimation parameter with units of 100-mile^{-1}.

The speed estimation parameter, g is often regarded as a constant that converts the occupancy into density, and the space mean speed is then calculated by the fundamental relationship between volume, density, and space mean speed. Because both traffic volume and lane occupancy are direct measurements from single loops, and T is a known variable from the system configuration, assuming a constant value of g for speed estimation with Equation (2-1) is simple and has been employed by many state departments of transportation. The Chicago Traffic Systems Center uses g = 1.90 (Aredonk, 1996), and WSDOT used g = 2.4 for a number of years until recently.

WSDOT currently uses nighttime traffic to calibrate *g* periodically, but this still results in a constant *g* between calibrations. Currently, it is common practice in most transportation agencies to use speed estimation algorithms that apply the speed formula in Equation (2-1) with a constant *g*. (In this report, such algorithms are called "traditional algorithms.") However, because the value of *g* is determined by the Mean Effective Vehicle Length (MEVL), which is approximately the sum of mean vehicle length and detector length as shown in Equation (2-2), it stays constant only when the MEVL does not change from interval to interval (Wang and Nihan, 2000):

$$g(i) = \frac{52.80}{MEVL(i)} \tag{2-2}$$

where MEVL is in feet. If vehicle composition changes with time, the *MEVL* will vary considerably from interval to interval, and use of a constant *g* is not appropriate.

A number of researchers have proposed speed estimation methods independent of Equation (2-1). Pushkar et al. (1994) utilized a cusp catastrophe theory model to estimate average speeds at a location and compared the results to those obtained from a dual-loop sensor at the same location. Petty et al. (1998) utilized a stochastic traffic model based on assigning a common probability distribution of travel times to vehicles arriving at an upstream point during a given interval. This method, however, depends on disaggregate loop data (1-second polling intervals were used in the study); thus, such a method is not applicable where even modest data aggregation is performed. Dailey (1999) used a Kalman filter to account for what he considered to be random error in the measurements. Although the speed estimates were reasonable, Coifman (2001) noted that the source of this random error was not well specified.

Sun and Ritchie (1999) used inductive waveform outputs from new loop detector cards combined with signal processing and statistical analysis to anonymously identify vehicles between detectors and estimate speed. They further demonstrated that the method is transferable without the need for recalibration; however, the method requires considerable investment to update the loop hardware and is thus not feasible for existing installations. Coifman (2001) used an exponential filtering method that could be implemented in a type 170 controller to estimate speed. He also re-addressed the distinction between space mean speed and time mean speed and offered the possibility of examining dual-loop detector stations. However, with the notable exception of Coifman's exponential filter, all of the filtering and modeling methods discussed above suffer from some common drawbacks. Some require calibration at each collection site, while others make use of additional data not typically collected at single-loop stations.

Other researchers have focused on developing algorithms to avoid the speed estimation bias caused by using a constant *g*. Hellinga (2002) proposed an algorithm that uses dual-loop measured vehicle lengths to calculate *g* and applies the obtained *g* value to estimate speeds at adjacent single-loop stations. Because some dual-loop detectors are required, this algorithm is only suitable on freeways with mixed detectors of single loops and dual loops. Kwon et al. (2003) used an MEVL representative of short vehicles to estimate traffic speed across lanes and correlate those speeds to estimate truck volumes. This algorithm requires one truck-free lane (such as an HOV lane) and also imposes an assumption of cross-lane speed correlation. This assumption may not hold during congested periods when the speed in the high occupancy vehicle lane may be considerably different from those of neighboring lanes. Coifman et al. (2003) proposed

using the median vehicle length rather than the mean vehicle length to estimate speed by noting that the median is less sensitive to outliers than the mean and thus limits the impact of long vehicles on speed estimation. Wang and Nihan (2003) developed an algorithm to screen out intervals that may contain long vehicles from the speed calculation. Because passenger car lengths do not vary greatly, a constant *g* value corresponding to the average SV length can be used to estimate speed.

Relatively little work has been done to identify LVs by using single-loop data. Several of the previously discussed methods can also produce LV volume estimates. Sun and Ritchie (1999) utilized waveforms to identify LVs; however, as mentioned before, few currently deployed loop detectors can produce such waveform data. The method developed by Kwon et al. (2003) estimates LV volumes as well, but also relies on the assumption of cross-lane speed correlation, which may fail during congested periods. Cherrett et al. (2000) used the interval average occupancy per vehicle to identify LVs at speeds as low as 15 km/h. Wang and Nihan (2003) developed a distance weighted Nearest Neighbor Decision rule based on long and short vehicle population distributions of lengths to obtain favorable LV volumes. The inherent nature of this classification rule seems well-suited to LV classification.

Once the mix of SVs and LVs is known for a particular time interval, the MEVL can be calculated. Then speed can be estimated by using Equation (2-1), and the *g* value can be calculated from the MEVL.

2.2 VEHICLE DETECTION AND CLASSIFICATION USING VIDEO IMAGE PROCESSING

Computer vision is not an entirely new concept for vehicle detection and classification; many agencies began investigating the possibilities of video detection 15

or more years ago. The first systems, however, were unable to function adequately under a variety of environmental conditions. Shadows affected detection, nighttime detection was troublesome, and poor weather obscured vehicles. Therefore, many agencies continued to use loop detector systems or considered other detection technologies, such as radar (Weber, 1999). Over the years, however, many improvements have been made as advances in computer technology and image processing algorithms have been applied in the traffic detection arena. Early video detection research (Michalopoulos 1991) at the University of Minnesota resulted in the Autoscope video detection systems that are widely used in today's traffic detection and surveillance operations around the world. This section provides a brief overview of the state of the art in computer vision for traffic applications, focusing on shadow removal and length-based classification techniques.

2.2.1 Shadow Removal Techniques for Traffic Applications

The majority of research on removal of shadows from images has been performed in the fields of computer science and electrical engineering. One of the earliest investigations in shadow removal was done by Scanlan et al. (1990). They split an image into square blocks and produced an image based on the mean intensity of each block. The median intensity of the mean values was then used as a basis for scaling all blocks below the median to the median value. The authors noted that this method is appropriate only for images where the objects of interest occupy the higher end of the intensity range. Thus, the method would not be suited for situations in which the objects of interest occupy the lower end of the intensity range (Fung et al., 2002). This method also introduces some loss of contrast and tends to cause "blocking" (Wang et al., 2004).

Gamba et al. (1997) built a shadow model based upon images from a monocular color image sequence. The authors noted that shadows in a scene interact with still portions of the scene and that these are more like each other than they are like the target objects of interest. With this in mind, they used the hue, luminosity, and saturation values to construct a reference image for the shadow model. The shadows present in the reference image were used as a model for moving cast shadows. However, because the reference image may not always contain enough still shadows to provide an accurate model, they also constructed a strip bitmap model to improve the shadow model. In this strip bitmap model, the image was split into a number of horizontal strips to be analyzed separately, since luminosity values change with respect to distance from the camera (distant shadows appear lighter than closer shadows). Although the number of misclassified pixels was low, the algorithm was only tested on one scene at a supermarket parking lot. Furthermore, there was an implicit assumption that shadows are cast on the same kind of surface, which may not hold true for a variety of outdoor scenes (Fung et al., 2002).

Gu et al. (2005) implemented a biological approach to shadow removal. Noting synchronous pulse bursts in the visual cortex of cats, they implemented a Pulse Coupled Neural Network (PCNN) to simulate this effect for the removal of shadows on the basis of optimization of the linking strength. The results indicated that shadows were satisfactorily removed for images that did not contain high degrees of noise.

Hsieh et al. (2004) performed shadow removal to improve the accuracy of a person-tracking system. Their shadow removal method was based on the assumption that shadows have less variation in chromaticity and luminance. The tracked area was

decomposed by a wavelet transform and projected onto low and high frequency components to identify areas of low frequency that were considered to be shadow. The algorithm was able to perform satisfactorily even when the tracked people wore colors similar to that of the background.

Recognizing that many shadow removal algorithms produce distorted and noisy results that misrepresent the shape of the original object, Xu et al. (2005) set out to fix these distortion errors. They presented a shadow removal algorithm based upon inspection of color and texture. The unique part of their work was the introduction of morphological operations upon the blobs remaining after shadow removal to reconstruct the shadow-removed object shape on the basis of the shape of the object before shadow removal. The algorithm performs well except in cases of very large cast shadows. Correcting the brightness threshold used in the paper to account for larger shadows would improve the results but would also introduce false positive shadow pixels.

Fung et al. (2002) proposed a statistical shadow removal algorithm based upon construction of a probability map called the Shadow Confidence Score (SCS). The score was based on investigation of luminance, chromaticity, and gradient density. The cast shadow was determined to be those regions with high SCS values that were outside of the convex hull of the vehicle edge. The algorithm was tested on a variety of vehicle types and colors in different lighting conditions and viewing angles; the algorithm achieved an error rate of 14 percent. Motorcycles and vehicles with color similar to the background caused the highest rates of error. In the case of smaller vehicles, the error could largely be attributed to the use of a convex hull to represent the object, since smaller vehicles and motorcycles have outlines that are not very well preserved by a convex hull.

Noting that the performance of traditional Bayesian Networks deteriorates with highly varying input data, Lo et al. (2003) developed an adaptive Bayesian Network to avoid the problems of their static counterparts. This was accomplished through the development of an efficient means to capture the variation in subsequent input images. This information was then used to adjust the network parameters. The performance was evaluated against a static Bayesian Network, and the adaptive network performed better.

Wang et al. (2004) proposed a three-step process for removing shadows from a foreground object obtained after subtraction of an image from a background image. The first step is illumination assessment, in which the foreground region is analyzed on the basis of pixel intensity and energy to determine whether it contains any shadow. If a shadow is suspected to exist on the basis of aggregate statistics of bright and dark pixels, the shadow detection step is performed. The direction of illumination is found via the Otsu method (Otsu, 1979) over the boundary pixels. Points near the boundary in the direction of illumination are sampled to derive shadow attributes. Object areas are recognized by subtracting the edge image of the background from the edge image of the foreground object. Areas with remaining edges are considered to be the object area. In the final step, the object is recovered by using information from the object area and shadow attributes to construct the object. Foreground pixels with intensity values greater than the background, or those with characteristics different from the shadow attributes, are preserved. To preserve self-shadow areas, where pixels have characteristics similar to those of the cast shadow, pixels close to the object area are also preserved. Finally, any holes in the object area are filled. Scant experimental results were provided, limiting the ability to evaluate this method. Furthermore, the method used to find the direction of

illumination may fail if the shadow has a halo effect at the edge (pixels of high intensity at the boundary of the shadow).

An excellent survey and evaluation of many moving-shadow removal algorithms can be found in Prati et al. (2003).

2.2.2 Length Classification Techniques for Traffic Applications

There has been considerable interest in vehicle detection via computer vision, especially in crash-avoidance systems and other driver assistance systems; comparatively, there has been much less interest in vehicle classification via computer vision. Nevertheless, several investigations into vehicle classification via computer vision have been conducted recently. Lai et al. (2001) demonstrated that vehicle dimension could indeed be accurately estimated from a single camera angle through the use of a set of coordinate mapping functions. Through the use of a shadow removal method (important to maintain true vehicle dimensions) and a convex hull to produce a vehicle mask, they were able to estimate vehicle lengths to within 10 percent in every instance. Their method, however, requires camera calibration to map image angles and pixels into real-world dimensions. Furthermore, few vehicle types were tested, and the algorithm was applied in only one location.

Gupte et al. (2002) performed similar work by tracking regions—using the fact that all motion occurs in the ground plane—to detect, track, and classify vehicles. Before vehicles can be counted and classified, the authors' program must determine the relationship between the tracked regions and vehicles (e.g., a vehicle may have several regions, or a region may have several vehicles). In a 20-minute trial of the program, 90 percent of all vehicles were properly detected and tracked, and 70 percent of those

vehicles were properly classified. Unfortunately, their work did not address problems associated with shadows, so application of the algorithm is limited at the current stage.

Hasegawa and Kanade (2005) developed a system capable of detecting and classifying moving objects by both type and color. Vehicles from a series of training images were identified by an operator to develop the characteristics associated with each object type. The features used were mostly geometric, including bounding box dimensions, the centroid coordinate, and the area of the background-subtracted area. Linear discrimination analysis and a weighted K-Nearest Neighbor rule were used to assign presented vehicles to an object type. The color of each object was identified in a similar manner. In a test of 180 presented objects, 91 percent were correctly identified. A major disadvantage of the system is the requirement for training images from the location of interest. Furthermore, although color information may be helpful for identification and tracking of the same vehicle between images, it is not clear that such information is of interest for data collection; there are few if any assumptions about color alone that can lead to reliable vehicle classification.

Rad and Jamzad (2005) developed a program to count and classify vehicles as well as identify the occurrence of lane-changes through tracking. Their approach utilized a background subtraction approach combined with morphological operations to identify moving vehicle regions. Bounding boxes were obtained for each vehicle, upon which an occlusion analysis and classification were based. Boxes with a narrow width were determined to be motorcycles or bicycles. However, the bounding box characteristics were not sufficient to identify buses and heavy vehicles, so it was assumed that vehicles with lower speeds were buses and heavy vehicles. The report did not explain whether

speed estimation was performed or obtained via another detection system. Furthermore, this assumption is easily violated, especially in congested situations. Although favorable results were reported, only region measurement, splitting, and losses in tracking were analyzed, while the accuracy of vehicle detection and classification were not measured.

Graettinger et al. (2005) used video data collected from an Autoscope Solo Pro commercial detection system to provide classifications corresponding to the 13 FHWA vehicle classes. Noting that the Autoscope system can only produce five distinct length classification categories, they applied a disaggregation model that is typically used in stochastic hydrology to produce finer rainfall estimates from yearly rainfall data. They demonstrated the ability to produce FHWA-compliant classifications from as few as two Autoscope-based length categories. The method was tested at one location and validated at four other sites. Ground truth data were obtained via axle counters, and an overall misclassification rate of 3.4 percent was achieved. Interestingly, the authors noted that accuracy decreased when a higher number of length categories within the Autoscope program was used, so typically the minimum of two classifications was used. Accuracy decreased notably when a generic model was used because of the large dependency upon mean volumes during model training. However, use of site-specific models would be less feasible because new models for each location would have to be developed.

The studies described above provided valuable insights into the video-based vehicle detection and classification problems addressed in this study.

PART II SPEED AND BIN-VOLUME ESTIMATES USING SINGLE-LOOP OUTPUTS

3.0 SINGLE-LOOP ALGORITHM DESIGN

In this study, we developed a region growing algorithm to filter the data of all intervals in a period to identify intervals containing only SVs. Note that the terms "period" and "interval" are used with significant distinction here. An *interval* indicates the duration of a single volume or occupancy measurement and is predetermined by the loop detection system (20 seconds for the WSDOT loops used in this study). The term *period* indicates the sum of interval times for the total number of intervals observed.

Once the SV-only intervals are identified, Equation (2-1) is applied by using a constant *g* value based upon the SV mean length, as reported by Wang and Nihan (2003). LV volumes are then estimated by using the Nearest Neighbor Decision rule proposed in the same study.

3.1 PROPERTIES OF VEHICLE LENGTH DISTRIBUTION

We used the vehicle length distribution findings reported in Wang and Nihan (2003) to address the problem of obtaining speed estimates from single-loop data. Using data from a dual-loop detector (ES-163R: MMS___T3) in lane 3 of southbound I-5 at NE 130th St. from May 3 to May 16, 1999, Wang and Nihan found that the vehicle length distribution was clearly bimodal, as illustrated in Figure 3-1. The bimodal distribution of vehicle length indicated that vehicles can be naturally divided into two classes, corresponding to the SV class and the LV class, according to their lengths. This vehicle length distribution feature was verified by Kwon et al. (2003). Upon separation of the population into two groups at a length of 40 ft (12.2 m), Wang and Nihan (2003)

regarded the two resulting sub-distributions representing the SV and LV groups as normally distributed. These SV and LV length distributions with the associated normal distribution curves are illustrated in Figure 3-2.

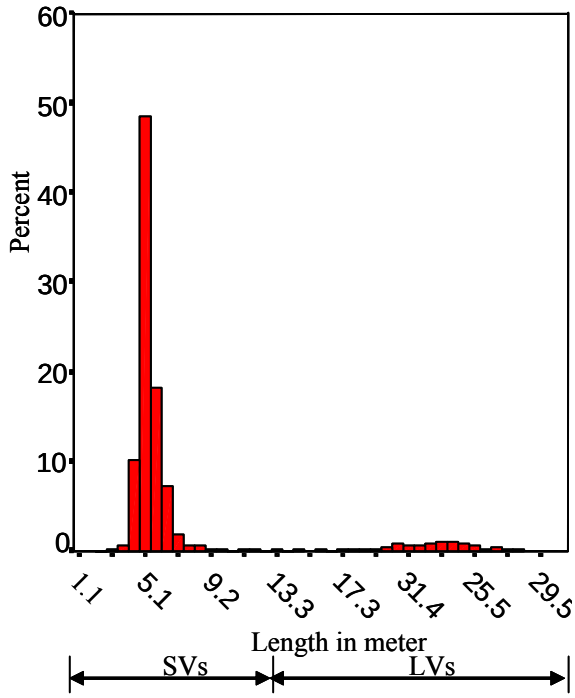

Figure 3-1: Length Distribution of Vehicles on Southbound I-5 (Wang and Nihan, 2003)

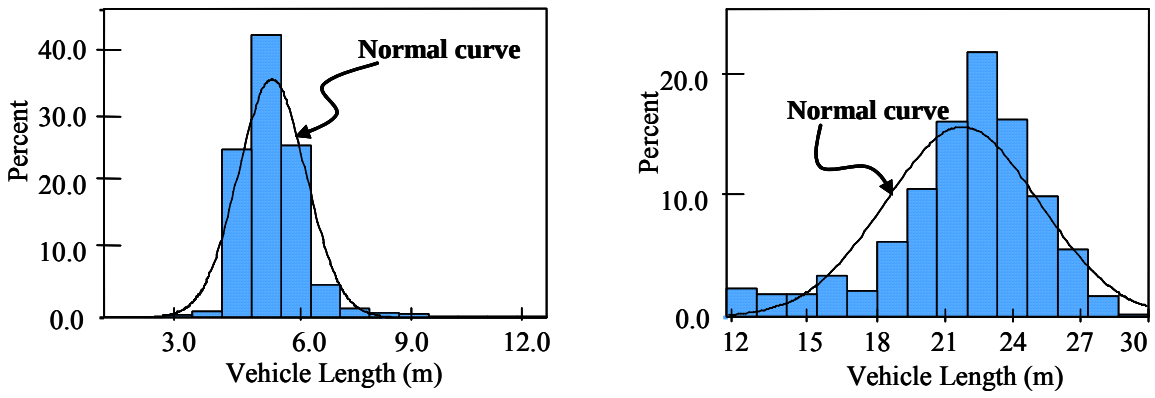

Figure 3-2: SV and LV Length Distributions with Normal Distribution Curves (Wang and Nihan, 2003)

Therefore, SV lengths are assumed to follow the $N(\mu_{sv}, \sigma_{sv}^2)$ distribution, and LV lengths to follow the $N(\mu_{lv}, \sigma_{lv}^2)$ distribution, where μ_{sv} and σ_{sv}^2 are the mean and variance of SV lengths, respectively, and μ_{lv} and σ_{lv}^2 are the mean and variance of LV lengths, respectively. The descriptive statistics for the two populations appear in Table 3-1. The standard deviation of SV lengths is σ_{SV} = 2.85 ft, about one fourth of that of LV lengths (σ_{LV} = 11.78 ft). This indicates that SV lengths vary narrowly in comparison to LV lengths. These vehicle length distribution features are used for separating intervals containing only SVs from those that contain LVs.

Table 3-1: Vehicle Length Distribution Statistics

	SV Class		LV Class	
	ft	(m)	ft	(m)
Mean	17.98	(5.48)	73.82	(22.5)
Std. Deviation	2.85	(0.87)	11.78	(3.59)
Minimum	6.00	(1.83)	40.00	(12.19)
Maximum	39.01	(11.89)	98.98	(30.17)
Observations	4443		472	

3.2 ALGORITHM DESIGN

3.2.1 Grouping Intervals

The design of our speed estimation algorithm is based on a revised "region growing" concept. Region growing is a technique traditionally used in image segmentation applications that allows computer vision systems to separate areas of an image into regions depending on criteria of interest, such as color or texture. Shapiro and Stockman (2001) stated that "a region grower begins at a position in an image and attempts to grow each region until the pixels being compared are too dissimilar to the

region to add them." The position at which region growing begins is known as the seed for the algorithm. This same idea can be used to discern between intervals containing only SVs and those containing LVs. One characteristic of region growing is that the statistics used for determining membership in a region are updated each time a new member is added to the region. Applying this concept to speed estimation, we first group *m* 20-second intervals into a period of length *m*/3 minutes (for example, if *m*=15 intervals, then the length of a period is 5 minutes). All the *m* interval data are then processed simultaneously to identify intervals with only SVs. Intervals with no vehicles present are eliminated from the analysis. The occupancy per vehicle (*O/V*) is calculated for each remaining interval, and the periods are sorted in order of ascending occupancy per vehicle to prepare for region growing.

Once the periods are sorted, it is assumed that the smallest non-zero *O/V* value consists of only SVs, which will serve as the seed for the region growing algorithm. Wang and Nihan (2003) found that an assumption that the smallest two non-zero *O/V* intervals contain only SVs was violated less than 3 percent of the time when 5-minute periods with the typical traffic composition (about 10 percent LVs) on I-5 were used. Therefore, the assumption that only the first interval contains only SVs would be violated even less frequently. The group occupancy per vehicle (*GOV*) is calculated by using the occupancy and volume measurements for all intervals already identified as being in the group (i.e., let interval *x* be the last identified interval in the group):

$$GOV = \frac{\sum_{i=1}^{x} O(i)}{\sum_{i=1}^{x} V(i)} \tag{3-1}$$

Then the occupancy per vehicle ratio ($\Delta_{O/V}$) of interval *x*+1 is calculated:

$$\Delta_{O/V} = \frac{O(x+1)/V(x+1)}{GOV} \tag{3-2}$$

The calculated $\Delta_{O/V}$ will be compared with a statistically determined parameter to decide whether interval x+1 should be accepted as part of the current group or a new group should be started. There is no limit on the number of groups it may generate. Under the assumption of constant speed over the m-interval period, the vehicle length distribution properties noted previously can be translated into occupancy distributions. Traditionally, the region growing model uses a hypothesis-testing t-statistic as a basis for inference of group membership at a specified confidence level. In this case, because the SV and LV length distributions are known to be normal, the threshold h is based on a normal distribution instead of the student-t distribution. The confidence level is chosen to equalize the probabilities of acceptance of an interval with LVs and rejection of an SV-only interval. Thus, the greatest amount by which the $\Delta_{O/V}$ value of an interval can differ from the mean while the interval is still accepted as an SV-only interval is given by:

$$h(i) = \frac{V(i)\left(\mu_{sv} + Z\sigma_{sv}/\sqrt{V(i)}\right)}{V(i)\cdot\mu_{sv}} = \frac{Z\sigma_{sv}}{\mu_{sv}\sqrt{V(i)}} + 1 \tag{3-3}$$

where:

μ_{sv} is the mean SV length

σ_{sv} is the standard deviation of SV lengths

Z is the Z-statistic corresponding to the chosen confidence level for a standard normal distribution

$V(i)$ is the number of vehicles (observations) in the interval.

For the vehicle distribution used in this report, the Z-statistic was chosen to equalize the probability of mis-assigning an SV as an LV with that of mis-assigning an

LV as an SV, which was found to be 3.817 standard deviations larger than the short vehicle mean.

One remaining factor, congestion, is taken into consideration before each interval is classified into a group. It is expected that, during congested periods, the mapping of interval occupancies onto the vehicle length distribution will be more prone to error. This is because, although the vehicle length distribution remains unchanged, interval occupancy levels will increase considerably during these periods, violating the constant speed assumption. For example, Wang and Nihan (2003) found that for a period length of m = 15 (5 minutes), actual speeds in the period varied by more than 15 percent in 46 out of 288 periods in the day, representing 16 percent of the periods. In particular, it is expected that the variances will be considerably affected by the increased variability of the data set. Accounting for these congested periods can help to relax the constant speed assumption and provide better results. Using loop occupancy as a surrogate for congestion, a brief study was conducted to measure the standard deviations of vehicle lengths at different loop occupancy levels. Loop event data were collected by the ALEDA (Cheevarunothai et al., 2005) system on southbound I-5 at 145th St on October 25-26, 2004. Figure 3-3 shows that congestion was clearly evident at loop occupancy levels of 20 percent and above, and the results presented in Table 3-2 indicate that at these occupancy levels, the standard deviations of length tended to be twice as large as those observed for low occupancy levels. Therefore, whenever the average loop occupancy for a period exceeds 20 percent, the Z-statistic in Equation (3-3) is doubled to account for the increased uncertainty in variance.

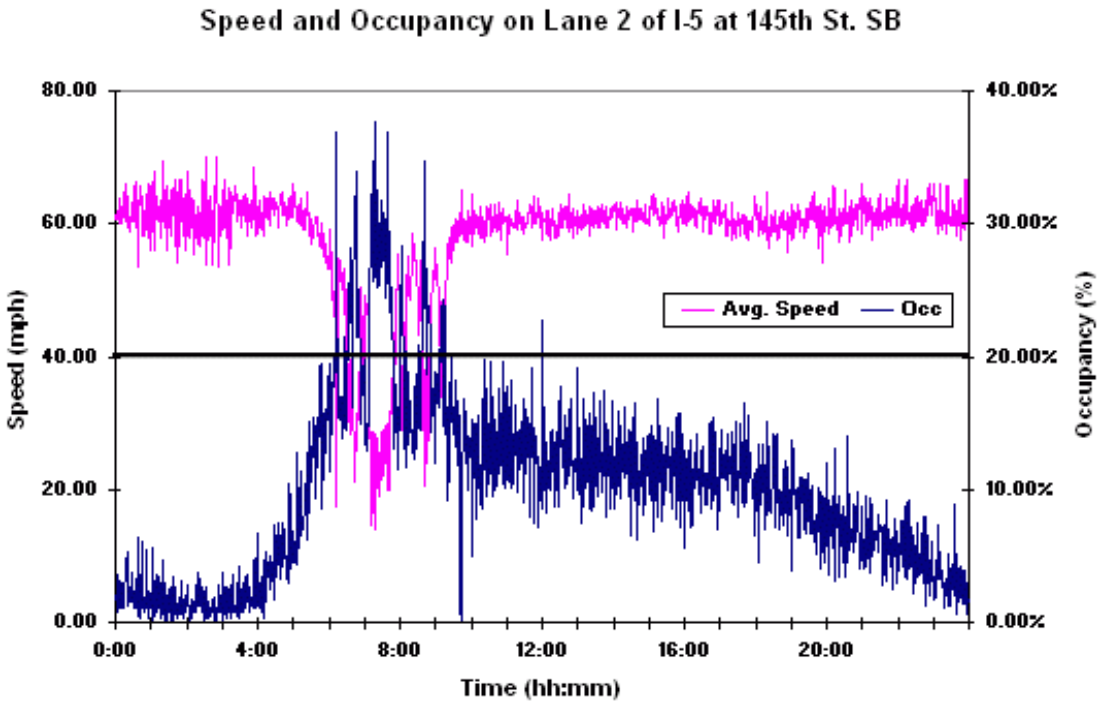

Figure 3-3: Congestion Occupancy Threshold

Table 3-2: Vehicle Length Distribution Statistics by Lane Occupancy Level

	Occupancy:	0-10%		10-15%		15-20%		20+%	
LANE 2	Observations	8088		11412		4502		2732	
	Minimum, ft (m)	38.82	(11.83)	12.26	(3.74)	11.63	(3.54)	8.62	(2.63)
	Maximum, ft (m)	87.27	(26.60)	100.08	(30.51)	77.37	(23.58)	69.93	(21.31)
	Median, ft (m)	63.42	(19.33)	58.34	(17.78)	53.74	(16.38)	30.39	(9.26)
	Average, ft (m)	61.44	(18.73)	59.84	(18.24)	53.41	(16.28)	32.27	(9.84)
	Std. Dev., ft (m)	4.74	(1.44)	5.13	(1.56)	8.09	(2.47)	9.47	(2.89)
	Multiplier			1.08		1.71		2.00	
LANE 3	Observations	10858		8515		4951		3068	
	Minimum, ft (m)	15.52	(4.73)	29.09	(8.87)	11.09	(3.38)	5.68	(1.73)
	Maximum, ft (m)	99.17	(30.23)	87.27	(26.60)	77.37	(23.58)	63.80	(19.44)
	Median, ft (m)	63.42	(19.33)	63.42	(19.33)	53.74	(16.38)	29.09	(8.87)
	Average, ft (m)	63.44	(19.34)	61.71	(18.81)	52.90	(16.12)	30.30	(9.24)
	Std. Dev., ft (m)	4.58	(1.40)	4.91	(1.50)	8.26	(2.52)	9.37	(2.85)
	Multiplier			1.07		1.80		2.04	
COMBINED	Observations	18946		19927		9453		5800	
	Minimum, ft (m)	15.52	(4.73)	12.26	(3.74)	11.09	(3.38)	5.68	(1.73)
	Maximum, ft (m)	99.17	(30.23)	100.08	(30.51)	77.37	(23.58)	69.93	(21.31)
	Median, ft (m)	63.42	(19.33)	58.34	(17.78)	53.74	(16.38)	30.30	(9.24)
	Average, ft (m)	62.59	(19.08)	60.64	(18.48)	53.14	(16.20)	31.23	(9.52)
	Std. Dev., ft (m)	4.75	(1.45)	5.12	(1.56)	8.18	(2.49)	9.46	(2.88)
	Multiplier			1.08		1.72		1.99	

To determine group membership, the occupancy per vehicle ratio is compared to the allowable relative difference calculated by Equation (3-3) as the threshold *h*. Whenever the $\Delta_{O/V}$ for an interval is less than the threshold *h* for that interval, the interval is considered to be a member of the group, and the *GOV* is updated. When an interval $\Delta_{O/V}$ exceeds the threshold, the group is closed, a new group is started, and the *GOV* for the new group is set to represent the current interval. The *GOV* for the new group is updated as additional intervals become members. In this manner, each interval in the period is assigned to a group. Figure 3-4 provides a flowchart of the algorithm.

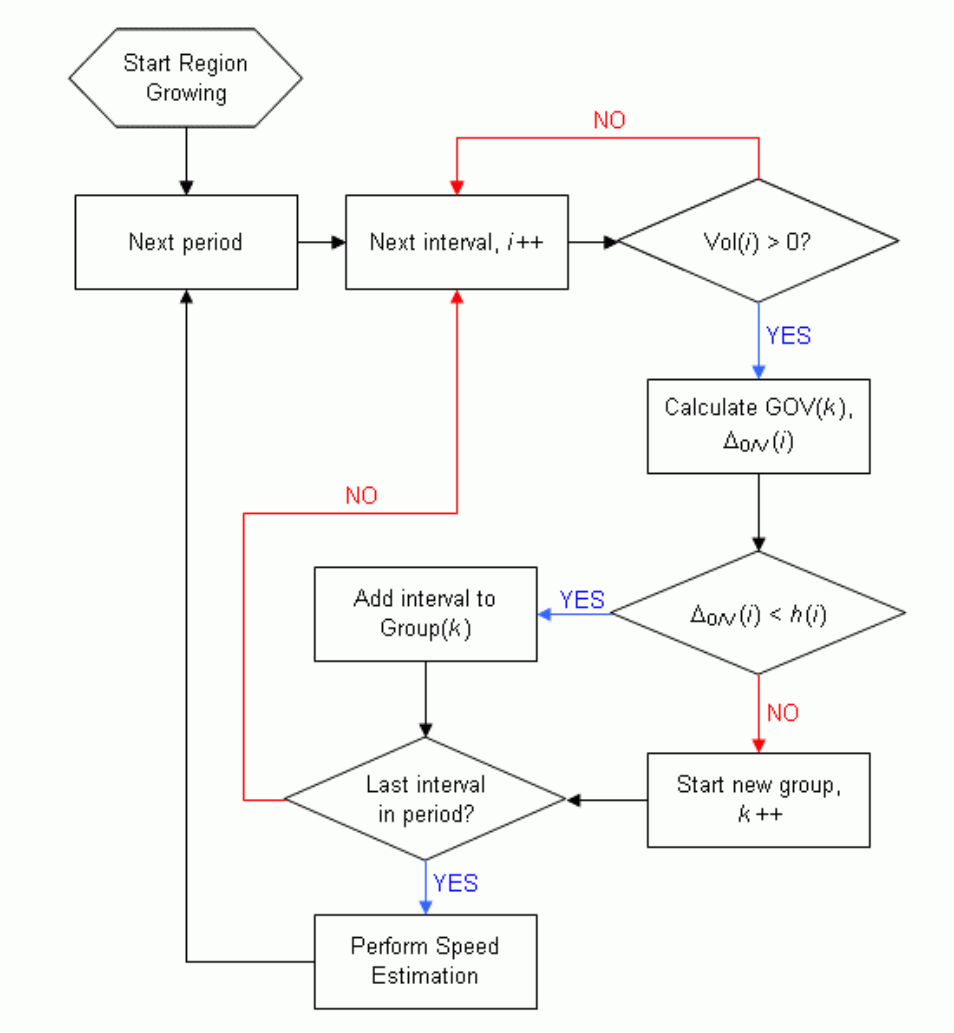

Figure 3-4: Single-Loop Region Growing Algorithm Flowchart

Figure 3-5 provides a visual example of region growing, with the identified groups colored differently. As indicated by the last column of the Excel worksheet in Figure 3-5, four groups are identified. The first group, colored in light green, corresponds to the SV-only group.

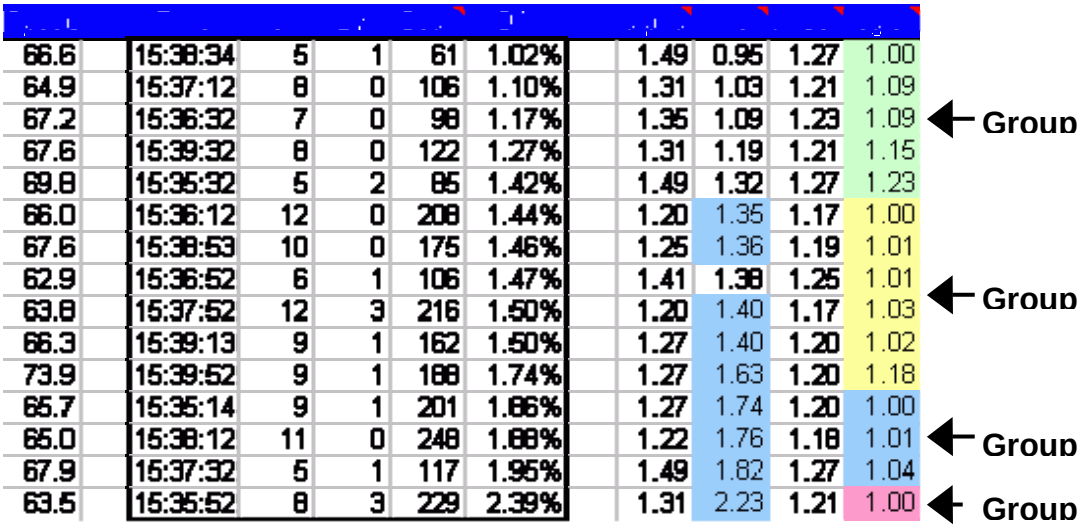

66.6	15:38:34	5	1	61	1.02%	1.49	0.95	1.27	1.00	
64.9	15:37:12	8	0	106	1.10%	1.31	1.03	1.21	1.09	
67.2	15:36:32	7	0	98	1.17%	1.35	1.09	1.23	1.09	← Group
67.6	15:39:32	8	0	122	1.27%	1.31	1.19	1.21	1.15	
69.8	15:35:32	5	2	85	1.42%	1.49	1.32	1.27	1.23	
66.0	15:36:12	12	0	208	1.44%	1.20	1.35	1.17	1.00	
67.6	15:38:53	10	0	175	1.46%	1.25	1.36	1.19	1.01	
62.9	15:36:52	6	1	106	1.47%	1.41	1.38	1.25	1.01	← Group
63.8	15:37:52	12	3	216	1.50%	1.20	1.40	1.17	1.03	
66.3	15:39:13	9	1	162	1.50%	1.27	1.40	1.20	1.02	
73.9	15:39:52	9	1	188	1.74%	1.27	1.63	1.20	1.18	
65.7	15:35:14	9	1	201	1.86%	1.27	1.74	1.20	1.00	
65.0	15:38:12	11	0	248	1.88%	1.22	1.76	1.18	1.01	← Group
67.9	15:37:32	5	1	117	1.95%	1.49	1.82	1.27	1.04	
63.5	15:35:52	8	3	229	2.39%	1.31	2.23	1.21	1.00	← Group

Figure 3-5: Interval Groups after Region Growing

3.2.2 Speed Estimation

Once the revised region growing algorithm has classified all intervals in the period, speed estimation can be performed quite easily. Because each interval has been classified into a group, all the intervals containing only short vehicles are in the first group. The volume and occupancy of this group is labeled V_{sv} and O_{sv}, respectively. The speed estimation parameter, g, is calculated in a manner similar to that of Equation (2-2), but using the mean short vehicle length, μ_{sv}, instead of the *MEVL* and a sensitivity correction parameter, β, as suggested by Wang and Nihan (2003):

$$g = \frac{52.80}{(\mu_{sv} + l_{loop}) \cdot \beta} \tag{3-6}$$

where l_{loop} is the loop detector length. A simple but effective way for calibrating β is to find a duration when traffic is free flowing. The space mean free flow speed is relatively stable over time. It can be calculated by using samples measured by a radar gun or simply estimated on the basis of speed limit and driving experience. By using the mean free flow speed and measurements of intervals with only SVs in the free flow duration, β can be calibrated through Equation (3-7),

$$\beta = \frac{\bar{s}_{ff} \cdot C}{\sum_{h=1}^{C} \frac{V_{sv}(h)}{O_{sv}(h)} \cdot (\mu_{sv} + l_{loop})} \tag{3-7}$$

where C is the number of intervals with only SVs in the selected free flow duration for β calibration; h is the index of intervals with only SVs; and $\bar{s}_{ff}$ is space-mean speed of free flow traffic at the station.

Once β has been calibrated, the algorithm is ready to provide dynamic traffic speed estimates for any time period. The estimated period space-mean speed, $\bar{s}_s$, is then calculated with Equation (3-8). Equation (3-8) is similar to Equation (2-1) except that a period SV volume and occupancy are used instead of an interval volume and occupancy.

$$\bar{s}_s = \frac{V_{sv}}{T \cdot O_{sv} \cdot g} \tag{3-8}$$

3.2.2 LV Volume Estimation

Although the revised region growing algorithm produces groups in addition to the SV-only group, there are no absolute mapping relationships between intervals in an LV-containing group and the number of LVs in an interval. This is because region growing depends on high membership similarity in each group to produce good results. While

intervals with no LVs are very similar in terms of average occupancy per vehicle, those with LVs are not. Consider an interval with one SV and one LV and an interval with ten SVs and one LV. Although both intervals have only one LV, the average occupancies per vehicle for each interval are quite different. Because the distance weighted Nearest Neighbor classification algorithm developed by Wang and Nihan (2003) is well suited to handle this situation, it was employed in this study to estimate LV volumes.

The Nearest Neighbor (NN) Decision rule is typically used to assign an unclassified sample to one of several predefined classification categories. The distance between the current sample and each of the predefined categories is calculated for comparison, and the category with the smallest distance to the current sample wins, i.e., the current sample is assigned to the nearest category. In this case, the predefined categories are all possible unique compositions of SVs and LVs. Because the maximal LV volume per interval observed on I-5 in the greater Seattle area is seven, the maximal number of predefined categories should not be more than eight. That is, for any interval k of period j, there should be no more than eight possible vehicle compositions, corresponding to LV numbers from zero to seven, respectively. If $V(i) < 7$, there are $N(i) + 1$ categories identified by LV numbers from 0 to $N(i)$. For example, if only four vehicles are detected in the interval (i.e., $N(j) = 4$), then the following five predefined categories can be assigned to: (4 SVs, 0 LV), (3 SVs, 1 LV), (2 SVs, 2 LVs), (1 SV, 3 LVs) and (0 SV, 4 LVs).

The vehicle composition in interval k is considered an unclassified observation. Its measurable feature is represented by its MEVL, $\bar{l}(k)$, calculated as follows

$$\bar{l}(k) = \frac{O(k) \cdot \bar{s}_s}{V(k) \cdot \beta} \tag{3-9}$$

As mentioned earlier, we assume that LV lengths and SV lengths follow the $N(\mu_{lv},\ \sigma_{lv}^2)$ and the $N(\mu_{sv},\ \sigma_{sv}^2)$ distributions, respectively. Because vehicle composition for an interval is an independent variable, the distribution of the mean vehicle length for a category with x LVs (where $0 \le x \le \min(7,\ V(k))$ can be determined as $N(\mu_x(x),\ \sigma_x^2(k))$, where

$$\mu_x(k) = \frac{(V(k)-x)\mu_{sv} + x\mu_{lv}}{V(k)} \tag{3-10}$$

$$\sigma_x^2(k) = \frac{(V(k)-x)\sigma_{sv}^2 + x\sigma_{lv}^2}{V^2(k)} \tag{3-11}$$

The similarity between the unclassified observation and the predefined category with x LVs is measured by the distance calculated by Equation (3-12).

$$d_x(k) = \left| \frac{\bar{l}(k) - l_{loop} - \mu_x(k)}{\sigma_x(k)} \right| \qquad \textit{for } x = 0, 1, \ldots, \min(V(k), 7) \tag{3-12}$$

Equation (3-12) converts variable $\bar{l}_k(j) - l_{loop}$ (mean vehicle length) into a standardized variable (a variable that follows the $N(0, 1)$ distribution) $d_x(k)$, which represents the distance to the origin. The smaller the $d_x(k)$, the greater the probability that the current interval contains x LVs. If

$$d_n(k) \le d_x(k) \qquad \textit{for } x = 0, 1, \ldots, \min(N_k(j), 7) \tag{3-13}$$

then we know that interval k belongs to the category that has n LVs. The LV number (n) and the SV number ($V(k) - n$) can be determined correspondingly.

3.3 ALGORITHM IMPLEMENTATION

The algorithm described in sections 3.1 and 3.2 was first implemented in Microsoft Excel with a Visual Basic for Applications (VBA) script. This implementation was used to develop the algorithm and produce the test results. For production uses, the algorithm was implemented in C# and the computer application was named single-loop Speed and Truck volume Estimator (ST-Estimator). The ST-Estimator system is a server-client type of system that uses the service provided by the loop_client application developed by the University of Washington (UW) Intelligent Transportation System (ITS) Research Program. The ST-Estimator allows users to collect real-time data in addition to archive analysis.

The loop_client application is a Unix program that disseminates lane occupancy and volume data collected by the WSDOT loop detection systems deployed in the Seattle area freeways (UW ITS Research Program, 1997). It posts loop detector measurements every 20 seconds on a designated server port (by default, it uses 9004). The ST-Estimator system connects to the loop_client server port by using the Transfer Control Protocol (TCP) for data download. Because loop_client does not support selective downloads, ST-Estimator takes in measurements of the most recent 20-second interval from all loop detectors. Selection is then made to store only user-specified loop data in a queue for real-time traffic speed and LV volume estimates.

Figure 3-6 provides a snapshot of the user interface when ST-Estimator is launched. All available loop stations are listed for users to select. If a station is double clicked, all loop sensors at this station are listed in the “Loop Sensors” window. A user

can then double-click a desired loop, and that loop will show up in the "Selected Loop" window. Only one loop can be selected at a time.

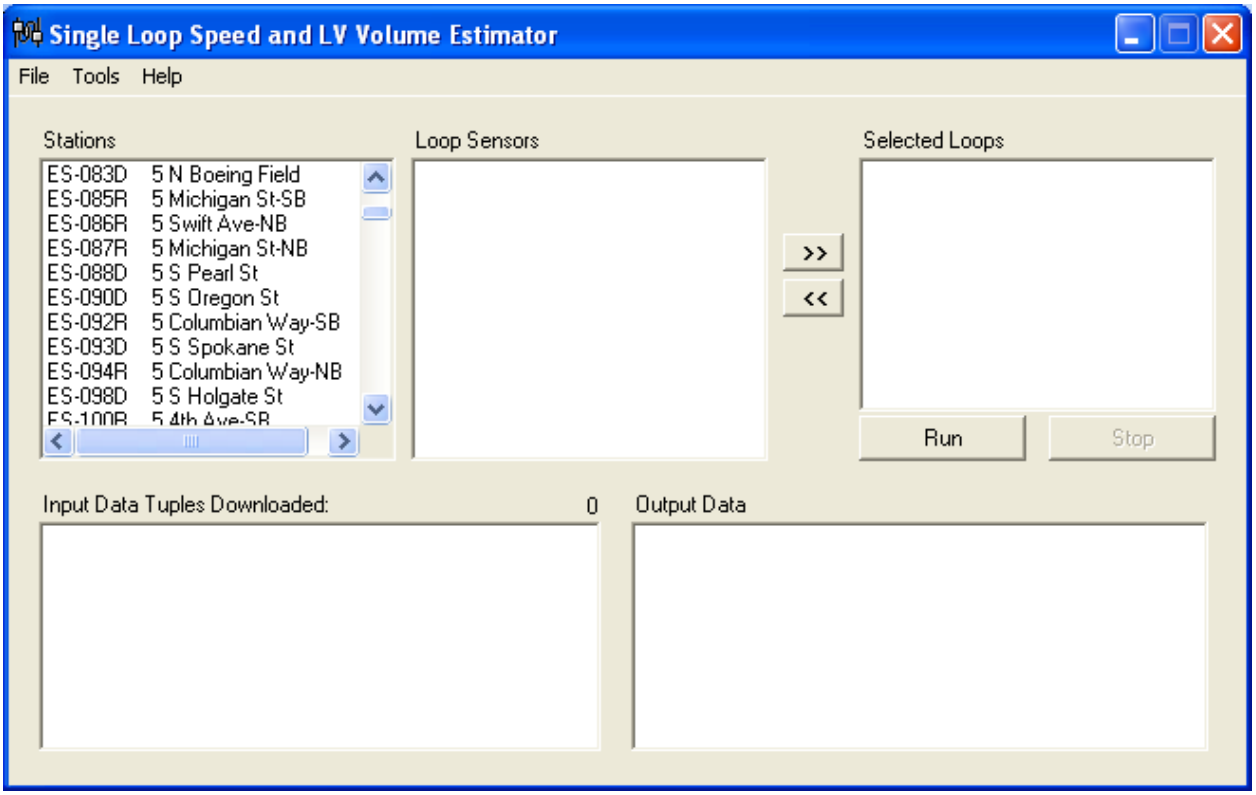

Figure 3-6: User Interface of the ST-Estimator System

Once a loop has been specified for speed and LV volume estimates, users can click the "Run" button to actuate the "Real Time Data" window. Loop detector name, location, vehicle count, lane occupancy, and estimated speed and LV number are shown together with the timestamp on this window. A snapshot of this window is shown in Figure 3-7.

System and algorithm parameters can be specified by users via a Program Settings interface (Figure 3-8). Users can modify the values for any program parameters under either the Basic tag or the Advanced tag of the interface. Furthermore, users can calibrate the loop sensitivity coefficient, β, by using night-time archive data and Equation (3-7).

With all the parameters specified, the ST-Estimator can provide speed and truck volume estimates in real time

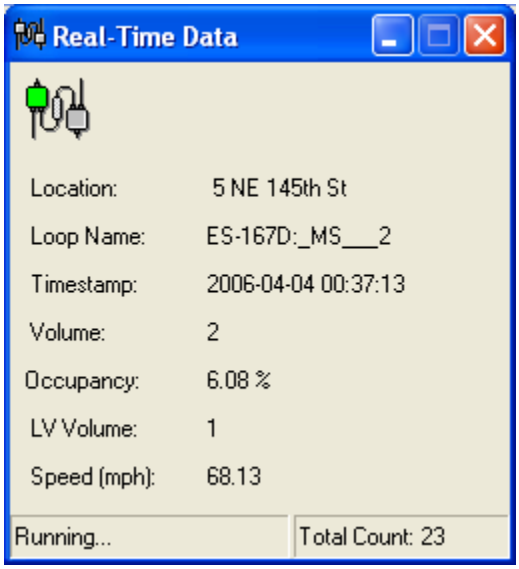

Figure 3-7: Real-Time Data Window of the ST-Estimator System

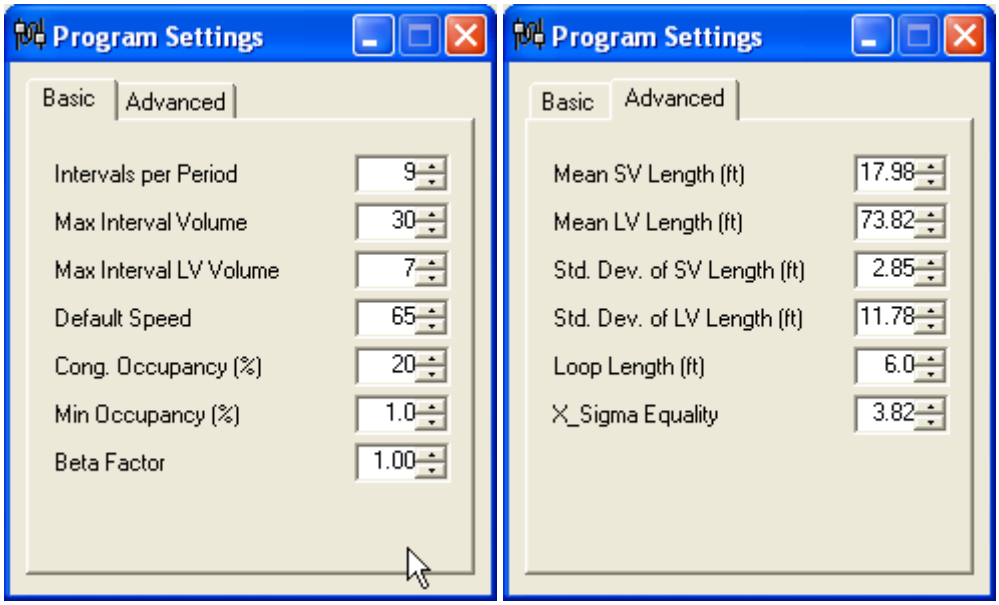

(a) Basic Program Settings (b) Advanced Program Settings

Figure 3-8: ST-Estimator's Program Settings Interface

4.0 SINGLE-LOOP ALGORITHM TESTS

4.1 TEST SITES

The single-loop speed and truck volume estimation algorithm implemented in ST-Estimator was tested by using data from three locations along I-5 in Seattle: station ES-167D at NE 145th Street (milepost 174.60), station ES-172R at the North Metro Base (milepost 175.50), and station ES-209D at 156th Street SW (milepost 184.49). All three stations are dual-loop stations, chosen so that the performance of the ST-Estimator could be compared to actual ground truth data recorded by the dual-loop detectors. Care was taken to select dual-loop stations that were functioning properly.

Twenty-four hour data (0:00-24:00) were collected at each station. These data are available for download from the Transportation Data Acquisition and Distribution (TDAD) website at the University of Washington (http://www.its.washington.edu/tdad/tdad_top.html). Descriptive statistics of the interval volumes for each location are tabulated in Table 4-1.

Table 4-1: Site Information and Interval Vehicle Volume Statistics

Station	ES-167D	ES-172R	ES-209D
Loop Code	_MS___2	MMS___2	_MN___2
Collection Date	17-May-05	25-May-05	18-May-05
Minimum Volume	0	0	0
Maximum Volume	18	18	18
Average Volume	6.55	7.11	6.96
Std. Deviation	3.77	3.94	3.99
M-Loop Volume	28295	30719	30046
S-Loop Volume	28273	30646	29577
T-Loop Volume	26800	30646	29149
M-Loop – S-Loop	22	73	469
M-Loop – T-Loop	1495	73	897
Dropped T-Loop Vol.	1473	0	428

4.2 TEST RESULTS AND DISCUSSION

The algorithm that directly applies single-loop measurements to Equation (2-1) for speed estimates by using a constant *g* is identified as the "traditional algorithm" in this report. The traditional algorithm and the proposed region growing algorithm were tested against ground truth data for periods of 9, 12, and 15 20-second intervals (3, 4, and 5 minutes, respectively). Graphs of the actual versus plotted values with R^2 values are provided in Figure 4-1, and a summary of the results is provided in Table 4-2.

A perfect estimation would result in all data points forming a line of slope 1.0 starting at the origin. Therefore, data points falling under the ideal line were underestimated speeds, and those above the line were overestimated speeds. The proposed algorithm, based on the revised region growing concept, clearly provided superior speed estimates.

The results of LV estimation are provided in Table 4-3. Comparisons are given in absolute differences for the entire day. Computation of more complex error measurements did not seem appropriate because LV volumes in general constituted less than 10 percent of the traffic at each location and, therefore, could be considered a somewhat "rare" event. Daily LV volume estimates were on average within 4.0 percent of the dual-loop estimated LV volumes.

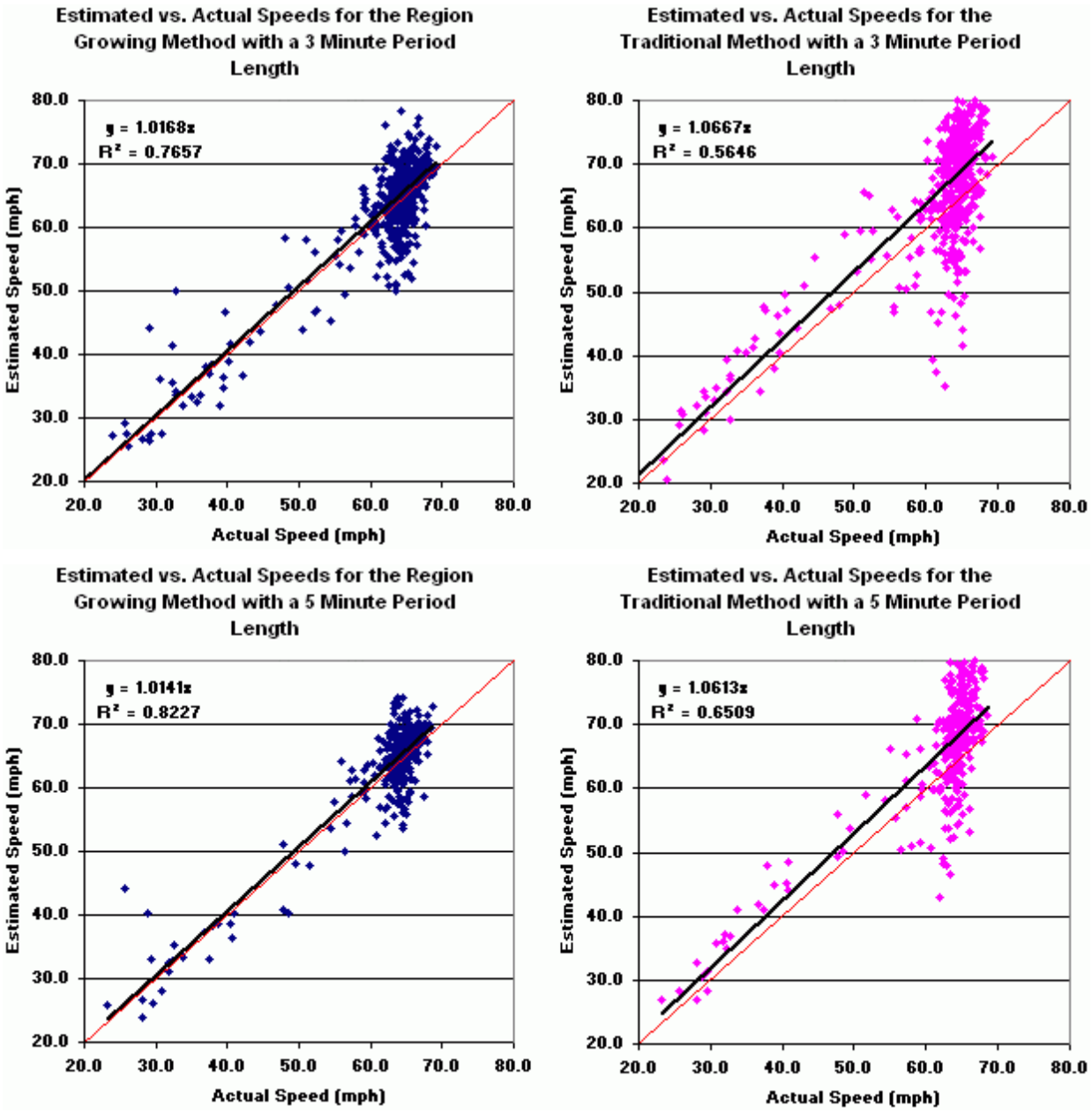

Figure 4-1: Estimated versus Actual Speeds for Region Growing and WSDOT Algorithms with Period Lengths of 3 and 5 Minutes on Lane 2 of Southbound I-5 at NE 145th St, May 17, 2005

Table 4-2: Summary of Speed Estimation Results

			Traditional Algorithm			Wang-Nihan Algorithm			Region Growing Algorithm		
Station & Loop Code	Loop Coeff. Beta	Period Length (min)	SSE	SSE / Period	Average % Error	SSE	SSE / Period	Average % Error	SSE	SSE / Period	Average % Error
ES-167D _MS___2	1.01	3	38504	80	**11.6%**	12593	26	**6.3%**	11432	24	**6.2%**
		4	24339	68	**10.7%**	6369	18	**5.5%**	7388	21	**5.9%**
		5	16471	57	**10.1%**	4124	14	**5.1%**	4741	16	**5.3%**
ES-172R MMS___2	0.92	3	34421	149	**11.1%**	16698	36	**7.2%**	10109	19	**6.2%**
		4	21293	59	**10.1%**	7208	20	**6.1%**	6275	17	**5.7%**
		5	14681	144	**9.4%**	4209	15	**5.4%**	3735	11	**5.0%**
ES-209D _MN___2	1.01	3	34650	255	**11.3%**	15265	34	**6.8%**	13421	25	**6.2%**
		4	21713	60	**10.4%**	9800	27	**6.5%**	8808	24	**5.8%**
		5	15815	257	**9.8%**	6550	25	**6.0%**	5309	17	**5.3%**

Table 4-3: Summary of LV Volume Estimation

Station & Loop Code	Period Length (min)	Dual-Loop LV Volume	Estimated LV Volume	Error	% Error
ES-167D _MS___2	3	2369	2315	-54	2.28%
	4	2369	2317	-52	2.20%
	5	2369	2285	-84	3.55%
ES-172R MMS___2	3	2566	2678	112	4.36%
	4	2566	2683	117	4.56%
	5	2566	2722	156	6.08%
ES-209D _MN___2	3	2630	2823	193	7.34%
	4	2630	2760	130	4.94%
	5	2630	2602	-28	1.06%

Because it is true that intervals containing LVs would naturally have a higher occupancy variance, one might question, on the basis of heteroskedasticity concerns, whether it is valid to use R^2 values as a measure of goodness-of-fit for speed estimates. However, the region growing algorithm does not require the homoskedasticity assumption that traditional linear regression requires. In fact, because intervals suspected to contain LVs are explicitly treated differently, the region growing algorithm does account for the heteroskedasticity inherent in the data. Thus, computing R^2 values on the

basis of speed estimates from the region growing model does not violate any classical econometric assumptions.

4.3 SINGLE-LOOP ALGORITHM TEST SUMMARY

The algorithm includes a revised region growing method for speed estimation and a method for LV volume estimation based on the Nearest Neighbor Decision rule approach. The revised region growing method identifies data intervals that do not contain any LVs for a particular time period. Volume and occupancy data from these intervals, together with a *g* factor derived from the mean of the SV population reported by Wang and Nihan (2003), are used to estimate average vehicle speed for the period. This speed is then used in a distance-weighted Nearest Neighbor routine to estimate the number of LVs present in each interval. The algorithm outperformed the traditional algorithm even when the value for the parameter *g* used in the traditional algorithm was calibrated with night-time data.

Further improvements to the proposed algorithm can be addressed in future research studies. For example, the algorithm's performance should be tested at the onset and dissipation of congested periods, when the constant average speed assumption is clearly violated. Also, the underlying vehicle distributions used in the proposed algorithm should be tested for spatial and temporal transferability to ensure validity in applying the algorithm to other testing locations.

PART III VIDEO IMAGE PROCESSING FOR VEHICLE DETECTION AND CLASSIFICATION

5.0 VIDEO RESEARCH APPROACH

To better utilize video equipment available to the majority of traffic systems management centers, we propose a simple yet effective vehicle detection and classification algorithm that uses un-calibrated surveillance video cameras to collect SV and LV volumes for individual roadway lanes. The research approach described here was split into four primary categories of investigation: background extraction, vehicle detection, shadow removal, and length-based classification. Details of each are discussed in the following sections.

5.1 BACKGROUND EXTRACTION

Typically, a computer vision-based detection system requires a background image that represents the base state of the area under observation. In the case of traffic detection, it is rarely possible to obtain an image of the observation area that does not contain any vehicles or other foreground objects. Therefore, it is necessary to extract the background image from the video stream itself. This is accomplished in an iterative fashion by using the pixels that make up an image. A grayscale image has only one value for each pixel that ranges from 0 and 255. A color image uses three color channels to represent a pixel's color. These three channels in the RGB color space are the Red channel (R), the Green channel (G), and the Blue channel (B). Each channel has a value from 0 through 255 that represents the amount of that color. When the median background extraction algorithm is applied to a color image, the median value of each color channel needs to be found for each color pixel. The intensity (or luminance) of a

color pixel is the value of grayscale converted from the R, G, and B color values by using Equation (5-1) (Shapiro and Stockman, 2001).

$$\text{Grayscale} = R * 0.30 + G * 0.59 + B * 0.11 \quad (5\text{-}1)$$

In this current study, the background image was obtained by constructing an image of the median value of each pixel from a collection of images:

$$bgd_{i,j} = median\left(img_{i,j}[n]\right) \quad (5\text{-}2)$$

where:

$bgd_{i,j}$ is the background image pixel value
$img_{i,j}$ is an array of image pixel values
n is the number of pixel values in the array.

In this study, we used a frame rate of 12 frames per second (fps) for video image processing. To extract the background image, 15 images spaced 20 frames apart were employed. By using the median value, it was assumed that the background was predominant in the image sequence. Figure 5-1 shows a snapshot of a video scene and the extracted background image for that scene. For data collections in locations with higher volumes (which would tend to obscure the background to a greater degree), a background extraction based on the mode of each pixel would be preferable (Zheng et al., 2006). In high volume and congested situations where portions of the background are never visible, more advanced background estimations might be required.

(a) A Snapshot of a Video Scene (b) Extracted Background

Figure 5-1: An Example Video Scene and Its Background

5.2 VEHICLE DETECTION

One potential disadvantage of using the background subtraction technique for detecting vehicles is that because the background is not updated frequently, it does not account for rapid lighting changes in the scene (Cucchiara et al., 2003). Such effects are often caused by the entrance of a highly reflective vehicle, such as a large white truck, into the scene. Before vehicles can be detected, these environmental illumination effects must be accounted for. In this current study, correction for environmental illumination effects was accomplished by using an automatic gain control (AGC). The AGC is a rectangular area that was placed in a part of the scene where the background was always visible (i.e., no vehicles were passing over the area). Thus, any changes in pixel intensities could be assumed to be due to environmental effects, since no physical objects had traversed the area. The average intensity change over this area from the background image could be determined and applied to the entire image to improve accuracy and avoid false vehicle detections:

$$\overline{\Delta int} = \frac{\sum_{A_{agf}} (bgint_{i,j} - imint_{i,j})}{A_{agc}} \tag{5-3}$$

where:

$\overline{\Delta int}$ is the average intensity difference over the AGC area

A_{agc} is the area of the AGC in number of pixels

$bgint_{i,j}$ represents pixel intensity in the background image on the interval $[0,1]$

$imint_{i,j}$ represents pixel intensity in the foreground (current) image on the interval $[0,1]$.

Vehicle detection was then performed with virtual detectors drawn by the user over the program scene. Each virtual detector consisted of a registration line, a detection line, and a longitudinal line, as illustrated in Figure 5-2.

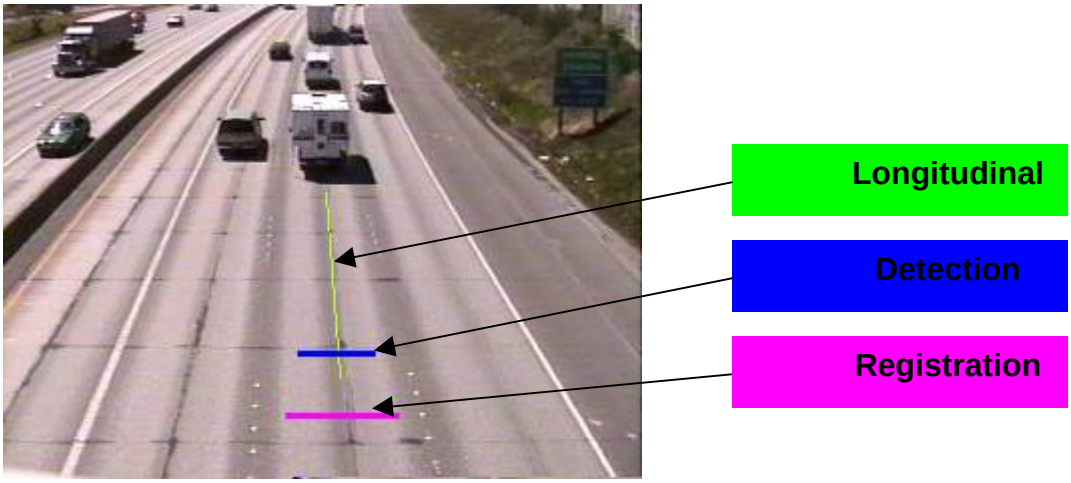

Figure 5-2: The Components of the Virtual Detector

Our vehicle detection algorithm first inspected for vehicles on the registration line:

$$\{p_{i,j} : p_{i,j} \in line\} : d_{i,j} = bgint_{i,j} - imint_{i,j} - \overline{\Delta int} \tag{5-4}$$

where:

$p_{i,j}$ represents a pixel location

$line$ represents the set of all pixels on the registration line

$d_{i,j}$ is the differenced pixel intensity on the interval $[0,1]$.

We then defined a set C that contained all differenced absolute pixel intensities greater than some threshold, t (in this study, a difference of 0.05 was used):

$$C = \left\{ d_{i,j} : \left| d_{i,j} \right| > t \right\} \tag{5-5}$$

If more than 30 percent of the members of a set *line* were also contained in the set C, we considered the line to be occupied by a vehicle. To present this fact graphically to the user, the color of the registration line was changed from green to magenta as a visual cue after each detected vehicle.

Once detected, each vehicle was processed and classified in one of two ways: entrance detection or exit detection. In entrance detection, the vehicle is already over the detector when it crosses the registration line, and processing occurs when the registration line is first occupied; that is, no vehicle was present over the line in the previous frame. In exit detection, the vehicle is fully in the detector as it is leaving the registration line, and the vehicle is processed upon exiting the registration line; that is, a vehicle was present over the line in the previous frame.

When a vehicle was processed, the detection line was inspected for differences in a manner similar to that of the registration line inspection. In this case, however, the set C of locations of absolute pixel intensities greater than t were used as seed points for obtaining the vehicle region, *Reg*, the set of all simply connected pixels satisfying the set membership rule for C without the requirement that they lie on the line. The bounding box was then the rectangular coordinates that represented the minimum and maximum coordinates of the pixels in region *Reg*. Computation of the bounding box localized the area of interest and improved the computational efficiency of the algorithm. The area

within the bounding box was then passed on to the shadow removal routine and length classifier.

5.3 SHADOW REMOVAL

The bounding box generated by the vehicle detection step often includes any shadow associated with the vehicle of interest. In these cases, it is often necessary to remove this shadow to obtain the true vehicle dimension and avoid introducing bias into the length estimates. Below are presented investigations of several shadow removal algorithms, as well as the algorithm employed in this study.

5.3.1 Experiments of Several Shadow Removal Algorithms

To design a high performance shadow removal algorithm, several methods were investigated to perform shadow removal in real time. The first method involved a dual-pass application of the Otsu automatic thresholding method (Otsu, 1979) to the intensities of the detected foreground pixels. The first application of the Otsu method separated the pixels into high and low intensity populations. The high intensity population was considered to be the vehicle of interest. However, the low intensity population might have consisted of both shadow pixels cast by the vehicle as well as self-shadow areas on the vehicle that were hidden from direct illumination sources. To separate these two areas, a second thresholding of the lower intensity population was performed. Those pixels above the resultant threshold were considered to be self-shadow pixels, while those pixels occupying the absolute lowest pixel range were considered to be the cast shadow.

One of the primary advantages of this method is that it is computationally inexpensive. Figure 5-3 illustrates that although the method performed well for bright vehicles with dark cast shadows, it did not perform as well when darker vehicles were

considered. Notice that in the latter case, self shadow regions of the pickup truck were classified as shadow and subsequently replaced by pixels from the background. Although this problem could be mitigated by allowing only points connected to the exterior of the vehicle to be classified as shadow, the algorithm also did not perform well when the cast shadow was not uniform and not as dark. This is illustrated in Figure 5-4, which was taken when the altitude of the sun was low, resulting in shadows that may have occupied higher intensity ranges than the vehicle itself.

Figure 5-3: Otsu Method for Shadow Removal on a Bright Vehicle and a Dark Vehicle

A second attempt at shadow removal applied a region growing method to identify the shadow area. Because shadow areas are more homogeneous in terms of intensity than most vehicles, we tried a region growing method to identify the shadow region cast by a vehicle. In this method, the direction of the shadow was determined to identify beginning seed points for growth of the shadow. The seed characteristics were extracted from a sample shadow region specified by the user. This method performed very well when the shadows were very dark or on the asphalt pavement without remarkable cracks (Figure 5-5). However, when the shadows occupied the relatively higher intensity ranges in low-

angle illumination on aged concrete pavement, the region growing approach did not perform well (Figure 5-6).

(a) Original Image (b) Image after Shadow Removal

Figure 5-4: Otsu Method for Shadow Removal with a Non-Uniform Cast Shadow

(a) Original Image (b) Image after Shadow Removal

Figure 5-5: A Successful Example of the Region Growing Shadow Removal Method

(a) Original Image (b) Image after Shadow Removal

Figure 5-6: An Unsuccessful Example of the Region Growing Shadow Removal Method

5.3.2 Design of a Combined Shadow Removal Algorithm

The final approach for shadow removal used in this study was based on identification of the shadow area in the subtracted edge image of the foreground from the background. The first step in this approach was to determine the relative position of the shadow to the vehicle. An easier way to specify this is through a user's interactive input. The calibration user interface of the VVDC system provides users choices of shadow position relative to a vehicle: a vehicle's shadow is located at its (1) upper left, (2) left, (3) lower left, (4) upper right, (5) right, or (6) lower right. A user can select the relative position of shadow on the calibration user interface.

Another more general method is to determine the shadow position based on the position of the sun. This is possible because during daytime detection any cast shadows can be assumed to be generated by the sun. The position of the sun can be calculated by knowing the time of day and the approximate latitude and longitude of the location under study. The method used by Gronbeck (2004) was applied in this study. Once the sun's

location was known, the pan angle of the camera view with respect to due north was all that was necessary to calculate the direction of the shadow in the image:

$$\alpha = \theta_c - \theta_{azim} + \frac{\pi}{2} \tag{5-6}$$

where:

α = the image shadow angle in radians counterclockwise from the positive x-axis;
θ_c = the camera pan angle in radians counterclockwise from due north; and
θ_{azim} = the sun azimuth angle in radians counterclockwise from due south.

The next step was to produce an edge image of the vehicle by using the method developed by Canny (Canny, 1986):

$$edge_{pxq} = Canny(img_{pxq}) - Canny(bgd_{pxq}) \tag{5-7}$$

where:

$Canny(I)$ = the Canny edge image of image I
img_{pxq} = the foreground image framed by the bounding box
bgd_{pxq} = the background image framed by the bounding box
$edge_{pxq}$ = the difference edge image of foreground and background.

The background edge image was subtracted from the foreground image to eliminate edges present within the bounding box that were persistent in the background. The edge image was then dilated once to close any gaps in the edge lines. Dilation, erosion, closing, and opening are mathematical morphology operations used in image processing. More details about these operations are available in Shapiro and Stockman (2001). Figure 5-7 illustrates the resulting dilated edge image, along with images from intermediate steps.

(a) A Foreground Image

(b) The Corresponding Background Image

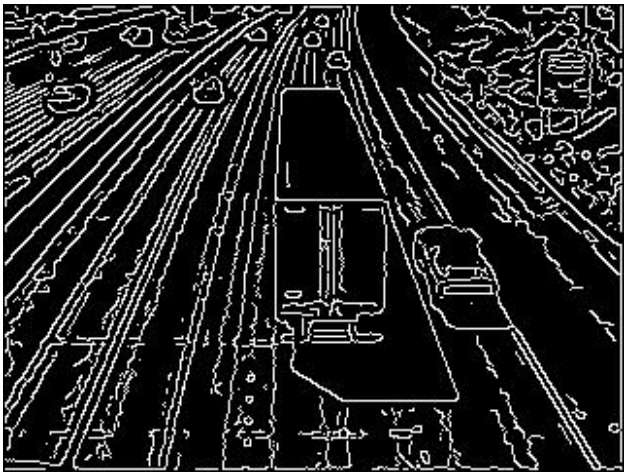

(c) The Edge Image of the Foreground

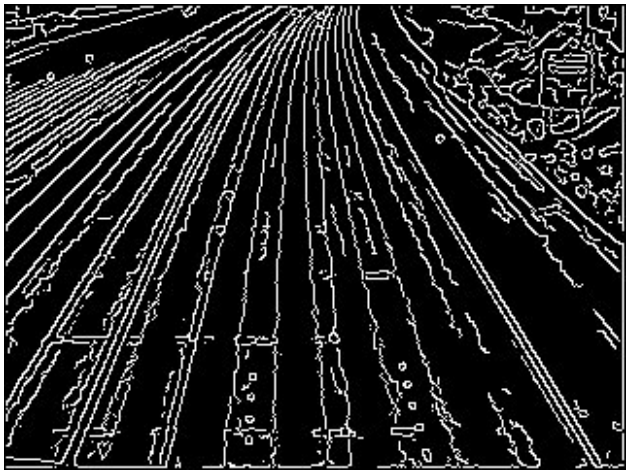

(d) The Edge Image of the Background

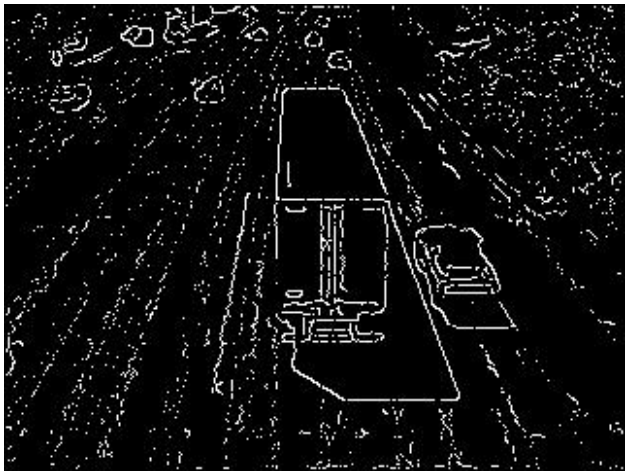

(e) The Subtracted Edge Image

(f) The Dilated Edge Image

Figure 5-7: Sample of Edge Imaging (Assuming the Bounding Box Includes the Entire Image)

The shadow location in the image was found in the following manner. First, a closing morphological operation was performed on the binary image to fill in holes in the vehicle region. The centroid of the binary mass was then found:

$$centroid = \left(\frac{\sum_{A} p_x}{A}, \frac{\sum_{A} p_y}{A} \right) \tag{5-8}$$

where:

p_x = the x-coordinate of a pixel in *Reg*

p_y = the y-coordinate of a pixel in *Reg*

A = the pixel area of the region *Reg*.

A line was then created from the centroid in the direction of the shadow angle. The point of intersection between this line and the outer edge of the region *Reg* was the point where the shadow was assumed to exist. The corresponding point in the edge image was used as a seed, and the shadow region, S ,was formed from the collection of all eight-connected points (in a 3×3 mask, not on an edge line). The binary region, V , representing the true vehicle could now be formed by subtracting the shadow region, S , from the region *Reg*:

$$V = R - S \tag{5-9}$$

A binary morphological opening operation was performed on the region V to remove any lingering loop around the shadow region. Figure 5-8 shows an example of a detected truck before and after shadow removal.

(a) Before Shadow Removal (b) After Shadow Removal

Figure 5-8: An Example of a Detected Truck Before and After Shadow Removal

5.4 LENGTH-BASED CLASSIFICATION

As mentioned in Section 3.1, the frequency distribution of vehicle lengths clearly indicated a bimodal distribution with two distinct peaks, one higher peak centered at about 18 ft (5 m), representing the concentration of SV lengths, and the other centered at about 74 ft (23 m) representing LV lengths. Note that the distributions were split at 40 ft (12.2 m), which corresponds to the boundary between bins 2 and 3 of the WSDOT vehicle classification system outlined in Table 1-1.

Trucks normally constitute less than 20 percent of traffic for major roadways in Washington State (WSDOT, 2002), which indicates that most of the detected vehicles on freeways are SVs. If a sufficient number of vehicle lengths are collected, the bimodal distribution can be applied to separate vehicles into SV and LV groups on the basis of relative length comparisons between vehicles. Relative comparisons to determine vehicle classification have been proven effective by Wang and Nihan (2003) in developing more accurate speed estimation for single-loop detectors. The method can be extended further by using the apparent pixel-based length of vehicles rather than the physical length. This

was feasible in the current study because the only desire was to classify vehicles by length, and it was not necessary to know the actual length of each vehicle, as long as it was properly classified. As soon as a vehicle exits the registration line, the length algorithm merely moves along the longitudinal line, counting the number of pixels as the pixel-based length of the vehicle. This ensures that the lengths of all the vehicles in a lane are measured at almost the same starting point, so that the measured vehicle lengths are comparable. Note that these are relative lengths, and a particular length measurement does not represent the actual length of the vehicle. In this manner, vehicles can be separated by length and classified without requiring camera calibration. This increases the flexibility and attractiveness of this mobile traffic detection system.

In the application, pixel-based vehicle lengths for each vehicle were obtained once the shadow had been removed from the vehicle. This vehicle length was simply the length along the longitudinal line that was occupied by the vehicle region V :

$$len = \sqrt{(e_x - s_x)^2 + (e_y - s_y)^2} \tag{5-10}$$

where:

s_x, s_y = the start coordinates of the line
e_x, e_y = the end coordinates of the line
len = the pixel-based length of the vehicle.

The pixel-based length of each vehicle was then compared with a threshold value to determine whether it belonged to the SV category or the LV category. Because a vehicle looks different in cameras with different lens and posture settings, the threshold value could not be a universal predetermined value.

The threshold value for each lane can be specified by users with the interactive interface of the VVDC system. The length of the longitudinal line of each virtual loop serves as the threshold. To specify the threshold accurately, a user can wait until a

representative vehicle shows up and then use the vehicle as a reference to draw the longitudinal line. Vehicles longer than the longitudinal line are assigned to the LV category. Specifying the length threshold this way provides users with the flexibility to collect classified vehicle volumes of desired lengths.

6.0 DEVELOPMENT OF THE VIDEO-BASED VEHICLE DETECTION AND CLASSIFICATION SYSTEM

This section describes the development of the VVDC system that implements the algorithm presented in Chapter 5.

6.1 SYSTEM ARCHITECTURE

The VVDC system comprises a WinTV-USB device (details for this device are available at http://www.hauppauge.com/html/usb_data.htm) and a personal computer. It is designed for both online and offline operations on a regular personal computer running Windows 2000 or Windows XP. The personal computer used for VVDC system development was a Dell Latitude D600 laptop computer with a Pentium M 1.6 GHz Central Computing Unit, 1-GB memory, and a 32-MB ATI Radeon 9000 video card. It ran the Windows XP Professional operating system.

The WinTV-USB device is used for digitizing live video signals. When the VVDC system is executed offline, it reads digitized video images from a storage media, and the WinTV-USB device is not necessary. For online operations, the VVDC system reads real-time images from the WinTV-USB device from the location where a live video signal source is connected. The live video source can be a video cassette player or a video camera. The components of the VVDC system and possible video data sources are shown in Figure 6-1.

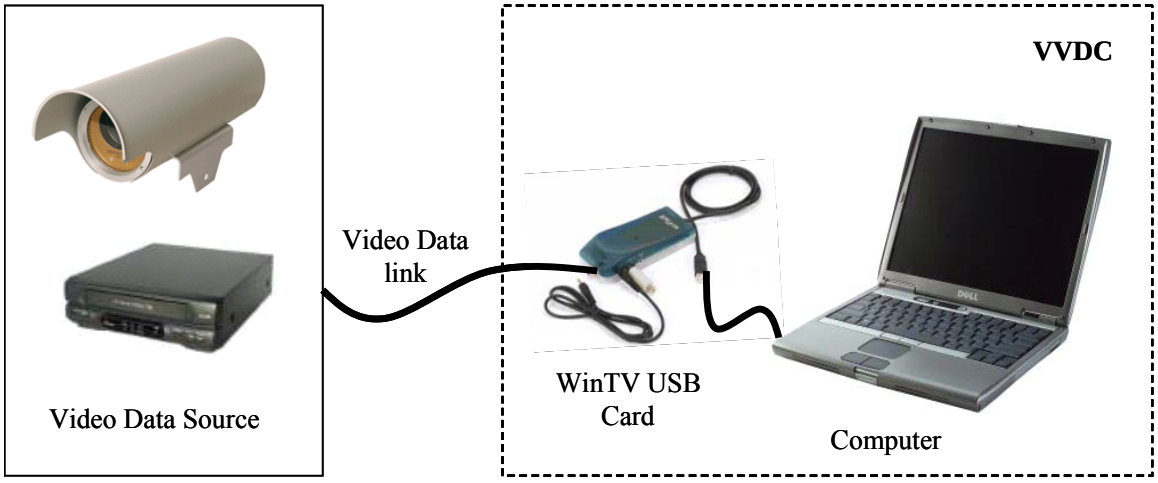

Figure 6-1: Components of the VVDC System

The software component of the VVDC system was written in the Microsoft Visual C# programming language. It has six modules: a live video capture module, a user input module, a background extraction module, a vehicle detection module, a shadow removal module, and a length-based classification module. The relationships among these modules are illustrated in Figure 6-2. Details of each module are described in the following sections.

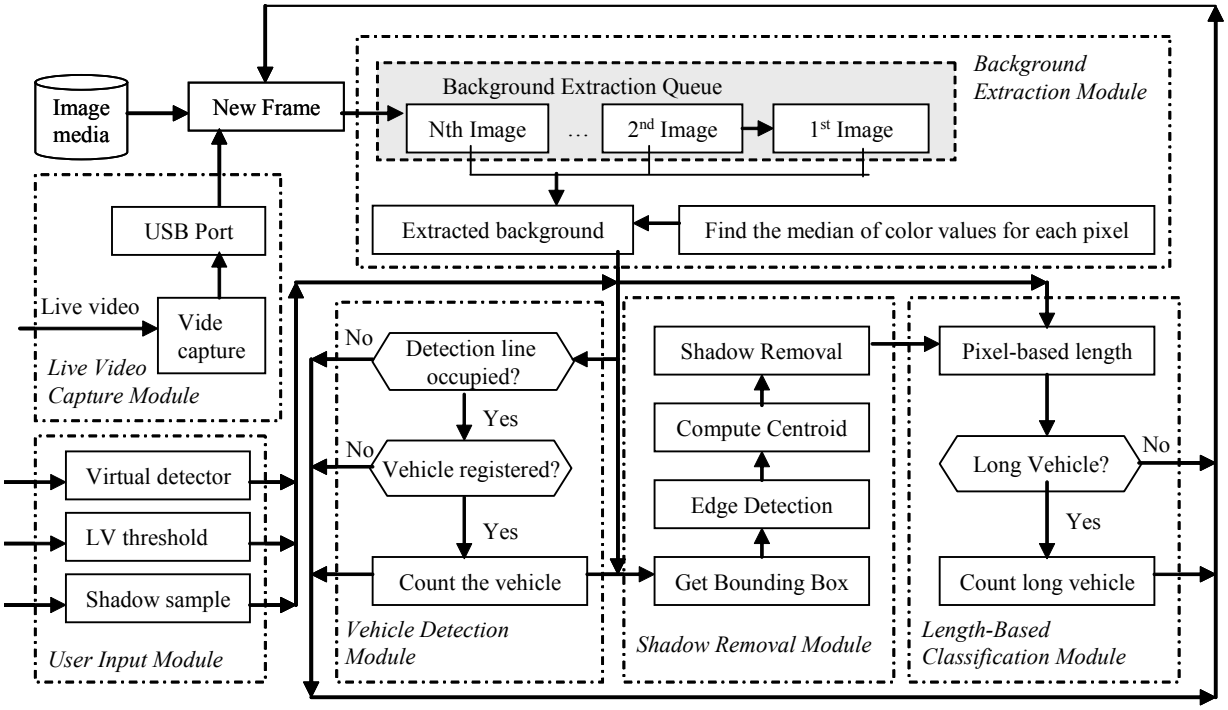

Figure 6-2: Flow Chart of the VVDC System

6.2 LIVE VIDEO CAPTURE MODULE

Because the image stream from each WSDOT camera location is multiplexed and transmitted via a fiber cable to the Traffic Systems Management Center (TSMC) for real-time traffic observation, control, guidance, and management, only an extension from the TSMC to the Smart Transportation Applications and Research Laboratory (STAR Lab) at the University of Washington was necessary. This link was established in September 2004 and enables access to any of the WSDOT surveillance cameras in the Puget Sound region. Only one video sequence can be transmitted over the feed at a time. A switch program developed by Dr. Dan Dailey in the Department of Electrical Engineering at the University of Washington is employed to switch the camera for display over the feed. Although this live video could be digitized into frames as the recorded video was, a goal

of this project was to use raw live video input directly in the program. This was accomplished via the live capture module.

As a plug and play system, the VVDC system has a live video capture module to digitize video images in real time for online applications. Live video signals can come from a surveillance video camera or a video cassette player. A WinTV-USB card produced by Hauppauge Digital, Inc. was used to implement this module. The WinTV-USB card is connected to a personal computer through a Universal Serial Bus (USB) port at one end and to the live video source at the other end through an S-video or composite adapter. This standard portable video device has a 125-channel, cable-ready TV tuner and is widely used for Internet video conferencing, TV-viewing, and image capture applications on computers. It is available at local electronic stores for approximately $100. The built-in features of the WinTV-USB device include video capture at variable rates and in different formats, adjustable image size, and changeable color configurations.

The live video capture module can produce digitized image streams in either the Joint Photographic Experts Group (JPEG) or the bit-mapped graphic (BMP) format and supports a capture rate of up to 30 frames per second (fps). Captured video images can be provided to other modules of the VVDC system for online analysis or can be stored in a folder for offline processing. For most roadway applications, 10 fps is sufficient to track vehicle movements. The VVDC system processes video frames at 12 fps for vehicle detection and classification, although our tests indicated that the system speed is able to handle 20 fps in real time. The image size used for the VVDC system is 320 by 240 pixels.

Although the WinTV USB device was chosen for capturing live video images, the VVDC system does not contain any code specific to this device. This means that the VVDC system can use any video capture devices supported by the Windows 2000 or Windows XP operating systems. The live video capture module uses Microsoft DirectX technology (Microsoft Inc., 2002) to search video sources connected to the computer. Once a video source has been identified, the VVDC system polls the digitized images at 12 fps by default. When more than one video source is available, the image stream from the first USB port is used as the default.

6.3 USER INPUT MODULE

Figure 6-3 illustrates the main user interface of the VVDC System, which consists of the current frame for analysis; the controls for folder selection, starting, stopping, and resetting the program; and an output window of detector data collected. Users can choose to open a directory where static images are stored for analysis or to proceed with live video processing, which assumes an available digitized video source on the computer. The field of view needs to be configured before data collection can proceed. The VVDC system provides interactive input functions for configuration. A snapshot of the interactive configuration interface is shown in Figure 6-4.

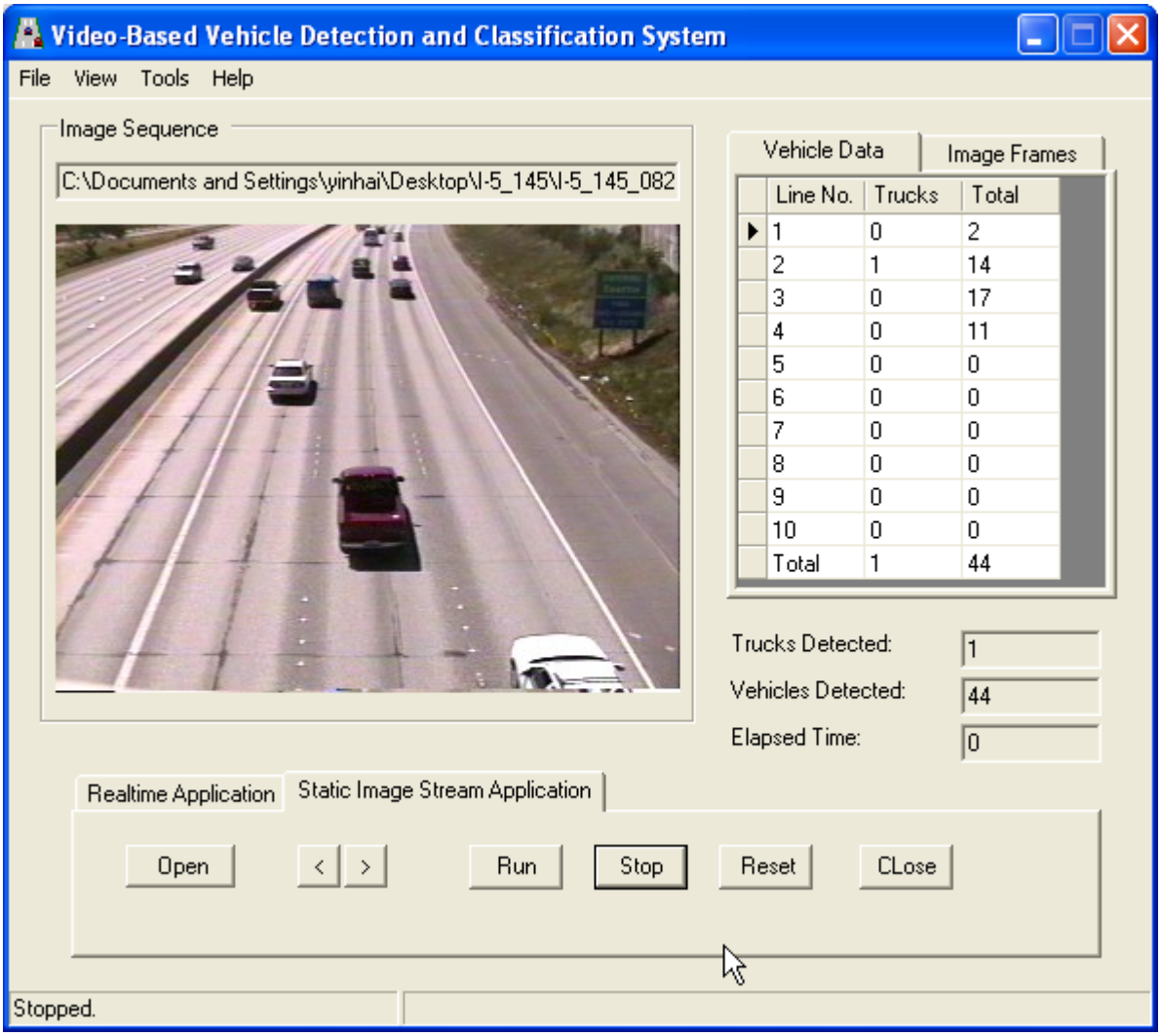

Figure 6-3: The Main User Interface of the VVDC System

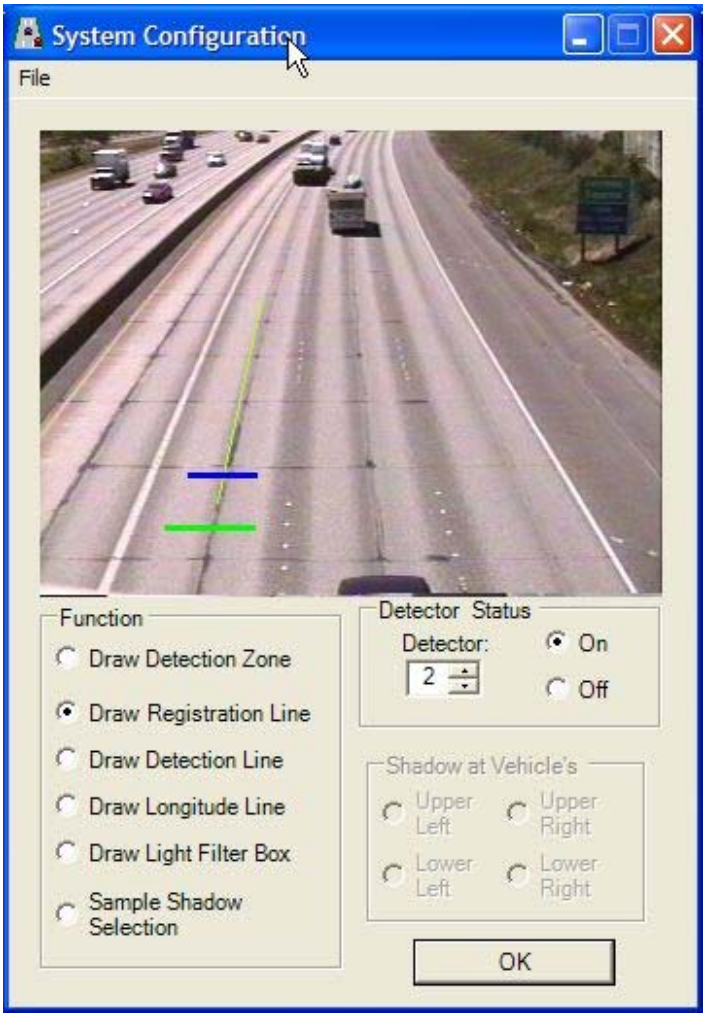

Figure 6-4: The Interactive Configuration Interface

The configuration process involves drawing the desired detectors, specifying the vehicle length threshold, selecting the AGC area (light filter box) and sample shadow zone, and specifying the relative position of shadow to a vehicle. Normally, one detector is needed for each lane. Detectors should be drawn at locations where vehicles are clearly visible with minimal occlusion problems. The longitudinal line for a detector serves as the threshold for separating SV and LV categories. The AGC box should be drawn at a location free of shadows and moving objects. A user can select a sample shadow zone that the VVDC system can use to extract statistical features of the current shadows and to

specify a vehicle's relative location to its shadow to facilitate the shadow removal process. As an alternative, a user can input the rough latitude and longitude of the data collection location and the pan angle of the camera view with respect to due north for the system to use in calculating the direction of the shadow. By default, the VVDC system uses the latitude and longitude of Seattle as the location for data collection. Configurations may also be saved and loaded to prevent having to reconfigure the same site twice. Once the site has been configured, the program is ready to perform data collection tasks.

6.4 BACKGROUND EXTRACTION MODULE

To run properly, the VVDC system requires a good quality background, at least at the virtual detector locations. The background extraction module used in the VVDC system employs the median background-extraction method described in Section 5.1. Depending on the roadway condition, it may take up to a minute to run the algorithm. To display the background extraction process visually to users, the module employs a task bar. Figure 6-5 shows a snapshot taken in the middle of a background extraction process. The green portion of the lower right bar indicates the percentage of the background extraction task completed.

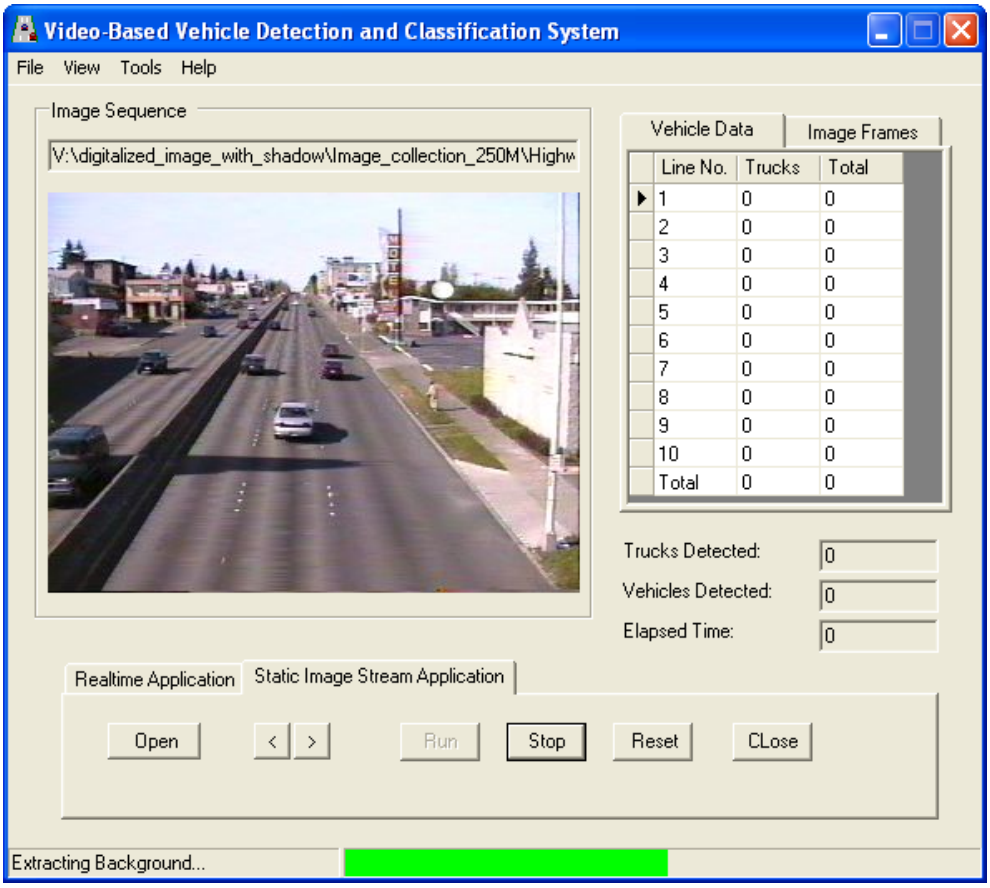

Figure 6-5: Background Extraction Process

After the background has been extracted, it can be viewed by using the View menu. Figure 6-6 shows the background extraction result from the process shown in Figure 6-5. If the extracted background image is not acceptable, the extraction process can be repeated until an acceptable background image is composed. A background image can be saved for future use.

Figure 6-6: Extracted Background Image

6.5 VEHICLE DETECTION MODULE

The processing loop of the VVDC system is based upon a timer that operates at a frame processing rate of 12 fps. During each cycle, a new image is obtained from a specified source. If the background image is not compiled, the image is passed to the background extraction module for background extraction. Otherwise, each image is processed according to the algorithm presented in Section 5.2 for vehicle detection.

The VVDC system detects vehicles at locations of virtual detectors. A virtual detector comprises a registration line (green), a detection line (blue), and a longitudinal line (green yellow). The distance between the registration line and the detection line must be shorter than the length of a short car and longer than the distance of vehicle movements between two consecutive frames.

The vehicle detection module scans the registration line and the detection line for every frame and compares the pixel values on the two lines to the corresponding background pixels. If the number of non-background pixels on the line exceeds a

threshold, then the line is marked as "on," which indicates that a vehicle is detected. When a vehicle is detected at the registration line, the color of the registration line changes to magenta so that users are aware of the fact that a vehicle has been detected. Similarly, when the detection line detects a vehicle, its color changes to yellow. A vehicle will not be counted until it exits the registration line and occupies the detection line. Such detection logic is designed to avoid over counting vehicles from minor camera vibrations and other video noises. Once the detection line has been occupied, the system keeps monitoring the registration line until the vehicle passes it. Then the VVDC system calls the shadow removal module to eliminate the cast shadow of the vehicle and the vehicle classification module to measure its pixel-represented length. Figure 6-7 shows a snapshot of the system when a vehicle is detected and classified. The program provides visual cues to users when vehicles are detected and processed. The program also logs the information of each detected vehicle in a text file.

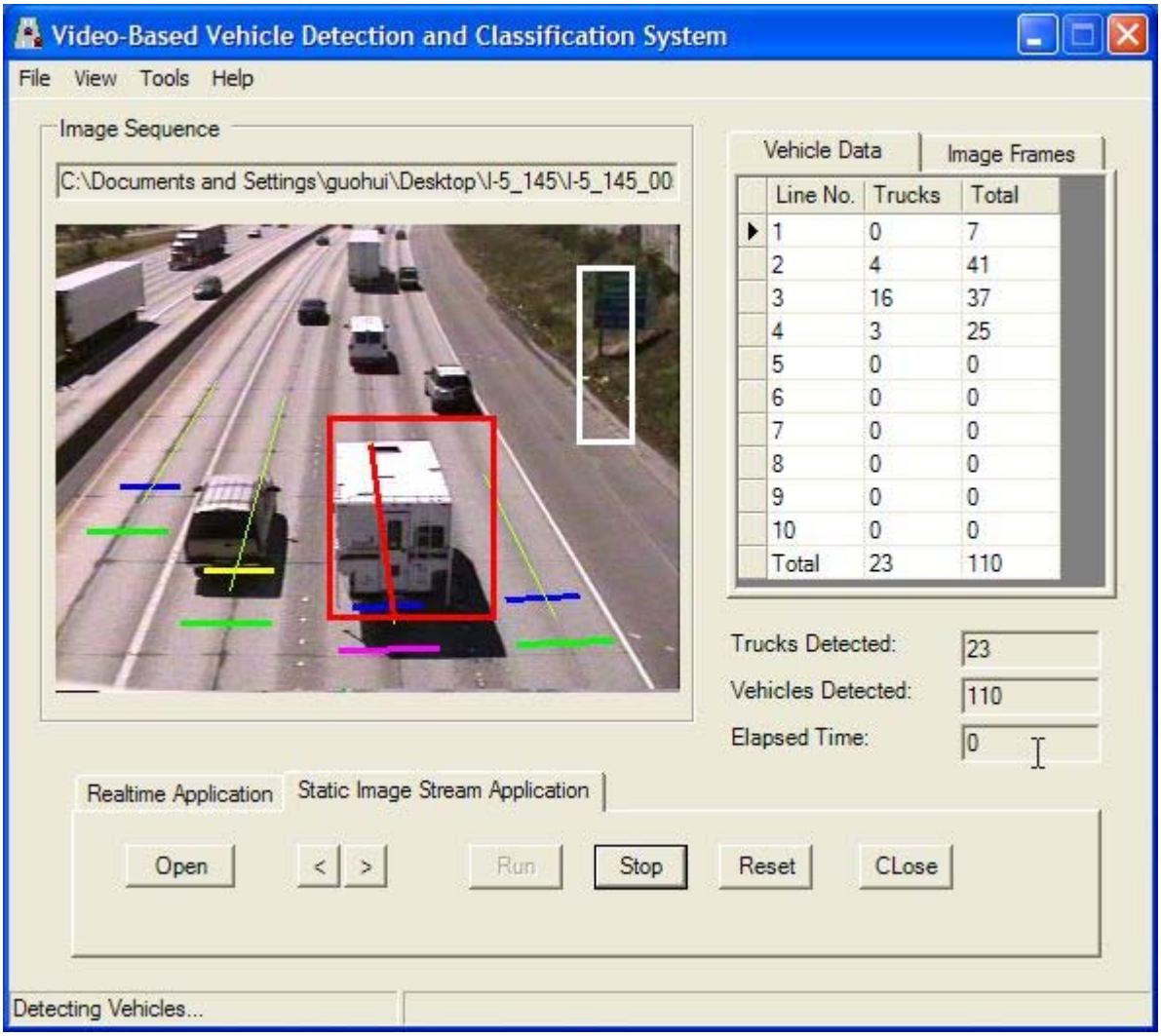

Figure 6-7: A Snapshot of the VVDC System When a Vehicle is Detected and Classified

6.6 SHADOW REMOVAL MODULE

Vehicle detection based on background subtraction can identify moving blobs on a video scene. Figure 6-8 shows an example image frame and its moving blobs detected by background subtraction. We can see that a vehicle's moving blob contains both the vehicle area and its cast shadow area. Without removing the shadow area, a vehicle's pixel-represented length may be exaggerated. More importantly, a lengthened shadow extended to adjacent lanes may cause false alarms and result in over counting problems.

Therefore, the shadow removal module is an important component in the VVDC system for accurate vehicle detection and classification.

(a) A Video Scene (b) Moving Blobs

Figure 6-8: Detection of Moving Blobs through Background Subtraction

The shadow removal module implements the algorithm described in Section 5.3. Although the authors employed a relatively simple algorithm for shadow identification and elimination, this process is still computationally expensive because of the edge detection and morphological operations involved. In the current implementation, the image region where edge detection and morphological operations are applied is limited to the area in each bounding box. This cuts down the computational time significantly and enables online applications of the VVDC system. Figure 6-9 illustrates the shadow removal process for the white van shown in Figure 6-8. If the vehicle region is smaller than a given threshold value after shadow removal, then the moving object will not be counted as a vehicle. After shadow removal, the vehicle region is passed to the vehicle classification module for length measurement and classification.

Figure 6-9: A Step by Step Illustration of the Shadow Removal Process (from left to right): (a) Original Image; (b) Bounding Box Area (Shown in Blue); (c) Detected Edges; (d) Shadow Identification; and (e) Shadow Removal.

6.7 VEHICLE CLASSIFICATION MODULE

The VVDC system classifies a vehicle into the SV or LV category on the basis of its pixel-represented length. After shadow removal, a moving object contains only its vehicle region. To calculate a vehicle's length in number of pixels, the intersecting points of the longitudinal line with the front and rear edges of the vehicle are needed. To find the intersecting points, a 5×3 mask is used to search along the longitudinal line. If nine of the fifteen pixels in the mask are non-background pixels, then the center point of the mask is considered to be on the vehicle body. The search starts from the crossing point of the longitudinal line and the detection line and ends when both the front and rear edges of the vehicle are found. Then a red line indicating the detected vehicle length is drawn within the bounding box to visually show the calculated vehicle length. If a vehicle's pixel-based length is longer than the LV threshold, the vehicle is assigned to the LV category. Otherwise, it is considered to be an SV. A snapshot of the VVDC system showing a calculated vehicle length is in Figure 6-7.

7.0 VVDC SYSTEM TESTS AND DISCUSSION

7.1 TEST CONDITIONS AND DATA

Because of the time constraints on this research project, the video image processing algorithm developed in this study has two limitations. First, it was designed for daytime detections only; the algorithm will not work under nighttime conditions. Second, the algorithm assumes that the space-headway is sufficient to prevent any vehicle pair from longitudinal occlusion. This means that the algorithm will not produce good results under congested conditions or when the camera angle is so flat that it produces significant longitudinal occlusion problems. Consequently, the system tests described below had to be performed under relatively restricted conditions.

The system tests were divided into two parts: two offline tests with archived video images and one online test with live video data. The two data sets for the offline tests were collected from different locations: one from southbound I-5 near the NE 145th Street over-crossing, shown in Figure 7-1, and the other from northbound SR 99 near the NE 41st Street over-crossing, shown in Figure 7-2. Both data sets were taken by a Canon L2 8-mm video camcorder. The I-5 test videotape was recorded between 11:30 AM and 12:30 PM on June 11, 1999. The SR 99 test videotape was taken from 4:00 PM to 5:00 PM on April 22, 1999. Twelve-minute video clips were extracted from both video tapes and digitized at a rate of 12 fps, resulting in 8,640 frames in each offline test data set.

Figure 7-1: Southbound I-5 Near the NE 145th Street Over-crossing

Figure 7-2: Northbound SR 99 Near the NE 41st Street Over-crossing

Online test data came from the live video feed link between the TSMC at the WSDOT and the STAR Lab at the University of Washington, shown in Figure 7-3 and introduced in Section 6.2. The camera selected for online testing was the camera shooting southbound I-5 near the NE 92nd Street over-crossing. A snapshot of this location is shown in Figure 7-4.

Figure 7-3: Live Video Display at the STAR Lab

Figure 7-4: Southbound I-5 Near the NE 92nd Street Over-crossing

7.2 OFFLINE TESTS

7.2.1 The I-5 Test Location

Given the camera location and the traffic volume at this site, vehicle occlusion was rare. Although the weather was sunny, the time of day during which the video stream was taken resulted in shadows that tended not to stray into other lanes. Thus, this image set provided an ideal test condition.

Table 7-1 shows the results of the VVDC system evaluation at this site, including manually observed results (ground-truth data), system operation results, and comparisons between the two. There was an overall detection error of only 1.06 percent, and trucks were properly identified approximately 94 percent of the time. These test results illustrated an encouraging performance by the VVDC system. Note, however, that even though the system test results for truck classification on lane 1 (the right-most lane) were the same as the observed results, this fact did not reflect perfect performance of the system. Comparisons to ground-truth data indicated that the system produced two mistakes: one truck was missed (a false dismissal), while another was double-counted (a false alarm). A brief summary of the system errors is provided in the footnotes of Table 7-1. Further error investigations were conducted manually, and these findings are described in Table 7-2.

Table 7-1: Offline Test Results from the I-5 Test Location

Time Period 12 minutes		Location: Southbound I-5 near the 145th Street Over-crossing									
		Lane 4		Lane 3		Lane 2		Lane 1		Subtotal	
Ground-Truth	# of Trucks	5		4		37		12		58	
	Total # of Vehicles	149		409		335		244		1136	
System Detected	# of Trucks	5		4		35		12		56	
	Total # of Vehicles	154		412		335		245		1146	
Error	# of Trucks	0[a]	0[b]	0	0	2	5.41%	2[c]	16.67%	4	6.89%
	Total # of Vehicles	5	3.36%	3	0.73%	0	0	3[d]	0.82%	11	1.06%

[a] absolute error, [b] relative percentage error, [c] one was missed and one was over-counted. [d] two cars missed and one truck over-counted.

Table 7-2: Error Causes for the Offline Test at the I-5 Test Location

Lane	Error descriptions	Explanations
Lane 1	1. One truck missed 2. One truck over-counted 3. Two vehicles missed	1. Same reason as that for Lane 2. 2. A truck that occupied both Lane 1 and Lane 2 was counted by both the Lane 1 and Lane 2 detectors. A snapshot of this truck is shown in Figure 7-5. 3. Two lane-changing vehicles did not trigger any of the two virtual loops. See the black car in the lower right corner of Figure 7-6 for example.
Lane 2	Two trucks missed	The two false dismissals were due to the fact that significant portions of the colors of the two trucks were too similar to the background color to have their lengths properly measured. Figure 7-7 shows one of the two trucks to illustrate the problem.
Lane 3	Three vehicles over-counted	Both Lane 3 and Lane 4 had false alarms. These false alarms were likely caused by the reflection of vehicle head lights from Northbound I-5 traffic.
Lane 4	Five vehicles over-counted	

Figure 7-5: A Truck Triggered Both Lane 1 and Lane 2 Detectors

Figure 7-6: A Lane-Changing Vehicle Missed by the VVDC System

Figure 7-7: A Misclassified Truck with the Color of the Bed Similar to the Background Color

7.2.2 The SR 99 Test Location

The late afternoon sun at this location caused significant cast shadows. This test data set was used to examine the adaptability and reliability of the VVDC system under a challenging situation. This testing location included three lanes on northbound SR 99. Vehicle shadows sometimes projected onto adjacent lanes, increasing the possibility of spurious vehicle counts. Additionally, at this location traffic flow was interrupted

periodically by signal control at the upstream intersection. Although the camera at this site was set reasonably high, periodic heavy traffic flow could also generate unexpected longitudinal occlusions. These factors hindered VVDC system performance.

The traffic condition at this site was representative of a more complex scenario. Selection of this site, therefore, enabled a performance evaluation of the VVDC system under complicated conditions. Table 7-3 summarizes the test results in the same manner as those presented in Table 7-1. The overall results were satisfactory, given that the test conditions were challenging. During the testing period the overall count error was less then 0.41 percent, and more than 93 percent of the trucks present were correctly recognized. The error details are provided in Table 7-4.

Table 7-3: Offline Test Results from the SR 99 Test Location

Time Period 12 minutes		Location: Northbound SR 99 near the NE 41st Street							
		Lane 3		Lane 2		Lane 1		Subtotal	
Ground-Truth	# of Trucks	8		7		15		30	
	Total # of Vehicles	270		244		192		706	
System Detected	# of Trucks	7		6		15		28	
	Total # of Vehicles	270[c]		245		194		709	
Error	# of Trucks	1[a]	12.5%[b]	1	14.28%	0	0	2	6.67%
	Total # of Vehicles	2	0.74%	1	0.41%	2	1.04%	5	0.41%

[a] absolute error, [b] relative percentage error, [c] one vehicle missed and one over-counted.

Table 7-4: Error Causes for the Offline Test on SR 99

Lane	Error descriptions	Explanations
Lanes 1-3	1. Four false alarms 2. One false dismissal	1. The four false alarms were caused by the reflections of sunlight on vehicle bodies. 2. A car that ran on the right shoulder did not trigger the detector on Lane 1. See Figure 7-8 for a snapshot of the vehicle.
Lane 2 and lane 3	Two trucks missed.	The false dismissals occurred because significant portions of the colors of two trucks were too similar to the background to have their lengths properly measured.

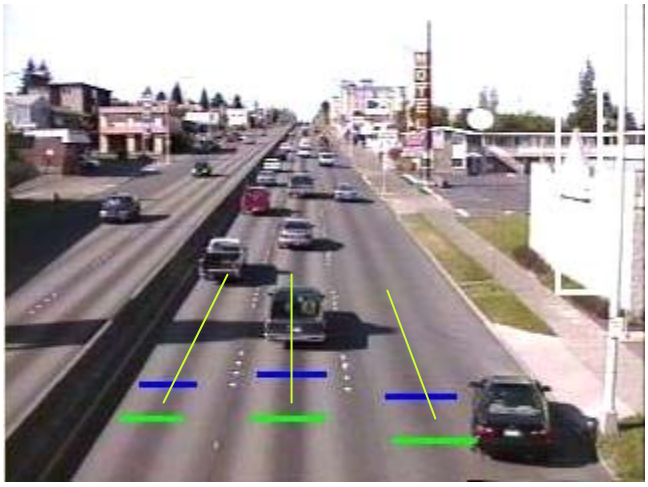

Figure 7-8: One Vehicle Driving on the Shoulder Did Not Trigger the Detector

7.3 ONLINE TEST

An online test was conducted with live video from the surveillance camera installed at southbound I-5 near the NE 92nd Street over-crossing. Live video signals were transmitted to the test computer via a fiber cable link between the WSDOT TSMC and the STAR Lab. Selection of this site enabled us to examine the robustness and reliability of the VVDC system when applied to live video images generated from a

typical surveillance camera. In comparison to an ideal test condition, the image quality of this data set was seriously affected by low-intensity rain and wet pavement. Although the image displacements resulting from the camera's vibration could be ignored, the moving objects were very small relative to the field of view. Additionally, reflections of vehicle lights on wet pavement became another remarkable source of disturbance. Therefore, this test was more challenging than the two offline tests described earlier.

The online test results for this location are summarized in Table 7-5. The overall accuracy of the vehicle count was 97.73 percent, and the truck count accuracy was 91.53 percent. The performance of the VVDC system was slightly lower in this online test than the offline tests. However, given that the test conditions were more complicated and challenging, the accuracy levels achieved during this online test were deemed satisfactory. In-depth reasons for the causes of each detection error are summarized in Table 7-6.

Table 7-5: Results of the Online Test at Southbound I-5 Near the NE 92nd Street Over-crossing

Time Period 12 minutes		Location: Southbound I-5 near the 92nd Street Over-crossing									
		Lane 4		Lane 3		Lane 2		Lane 1		Subtotal	
Ground-Truth	# of Trucks	13		36		5		5		59	
	Total # of Vehicles	388		378		380		170		1316	
System Detected	# of Trucks	14		37		6		5		62	
	Total # of Vehicles	397		387		389		173		1346	
Error	# of Trucks	1[a]	7.69%[b]	3[c]	8.33%	1	20%	0	0	5	8.47%
	Total # of Vehicles	9	2.31%	9	2.38%	9	2.36%	3	1.76%	30	2.27%

[a] absolute error, [b] relative percentage error, [c] one truck missed and two trucks double counted.

Table 7-6: Error Causes for the Online Test on Southbound I-5 Near the NE 92nd Street Over-crossing

Lane	Error descriptions	Explanations
Lanes 1-4	25 cars missed	Several lane-changing vehicles were missed at this location because they did not trigger any detectors. See Figure 7-9 for an example of such a vehicle. Our manual investigation also found that several vehicles were not detected when they passed over the virtual loops. This was probably because of random noises and the similarity of the vehicle colors to the background color. The camera at this location was mounted high to monitor all the 11 lanes. Consequently, vehicle regions were relatively small in comparison to those at other test locations. This made the detection more sensitive to random noises.
Lane 2	One container truck was missed	Please see Case 1 of Lane 3 for the cause of this error
Lane 3	1. One truck was missed 2. Two trucks were over-counted	1. The misclassified container truck is shown in Figure 7-10. The two containers were separated by a significant distance which prevented the length calculation algorithm from finding the front edge of the vehicle. 2. The VVDC system double counted two trucks because of the longitudinal occlusion of vehicles. Two separated SVs were detected as one LV. See Figure 7-11 for an example scenario of this problem.
Lane 4	One truck was missed	The error was caused by the similarity of the truck's appearance and the wet pavement. The system only recognized part of the truck and misclassified it as an SV.

Figure 7-9: A Lane-Changing Car Was Missed

Figure 7-10: A Gas Tanker Was Misclassified Because of the Large Distance between the Two Containers

Figure 7-11: Truck Over-Counts Due to Longitudinal Occlusion

7.4 VVDC SYSTEM TEST SUMMARY

Evaluation results from the three test locations were encouraging. The accuracy of vehicle counts was above 97 percent for all three tests. The effectiveness of the video

image processing method developed in this study was demonstrated. Both false alarms and false dismissals were found in the tests. False alarms in vehicle detection were mainly caused by wet pavement reflection. False dismissals were largely due to lane-changing vehicles or to vehicles driving on the shoulder without triggering the virtual sensors.

The accuracy of vehicle classification was lower than that of vehicle detection but was still in the acceptable range. The total truck count error was lower than 9 percent for all three tests. Two major causes of vehicle classification errors were longitudinal occlusion and inaccurate estimates of pixel-based length. When vehicles' moving blobs merge, the VVDC system cannot separate the connected blobs and hence overestimates vehicle length and over-counts trucks. For some combination trucks with two containers connected by a hitch, the vehicle length calculation algorithm failed to find the front edge of the vehicle and, therefore, misclassified it as two short vehicles. Trucks with a trailer or bed whose color was similar to the image background experienced similar problems.

The prototype VVDC system developed in this study cannot handle vehicle occlusions, severe camera vibrations, and head light reflection problems at the current stage. Depending on the frequency of these problems, the actual application results may vary from site to site.

PART IV PAIRED VIDEO AND SINGLE-LOOP SENSORS

Because WSDOT has both surveillance video cameras and single-loop detectors deployed along its major freeway corridors in the greater Seattle area, it was of practical interest to explore whether more accurate speed estimates could be achieved by combining video and single-loop data. At WSDOT's request, we also investigated the idea of pairing video and single-loop sensors for better speed estimates in this study.

8.0 PAIRED VIDEO AND SINGLE-LOOP SENSOR ALGORITHM

8.1 INTRODUCTION

As described in Section 2.1, a major challenge of calculating speed with Athol's algorithm, shown in Equation (2-1) (for readers' convenience, it is rewritten as Equation (8-1)), is determination of the *g* value for each time interval.

$$\overline{s_s}(i) = \frac{V(i)}{T \cdot O(i) \cdot g} \tag{8-1}$$

where i = time interval index
$\overline{s}_s$ = space mean speed in mph for each interval
V = vehicles per interval
O = lane occupancy in percentage of time the detector is occupied
T = the number of hours per interval
g = speed estimation parameter with units of 100-mile^{-1}.

When a noteworthy number of LVs is in the traffic stream, the MEVL may vary significantly from interval to interval. Without individual vehicle length information, it is very challenging to determining the *g* value for each time interval. However, if an interval does not contain any LVs, we can use the mean of the observed SV length distribution (Wang and Nihan, 2003) to approximate the average length of the vehicles detected in the interval because SV lengths vary narrowly, as described in Section 3.1.

Consequently, assuming that the average speeds of SVs and LVs in the same traffic stream are similar, a constant g value can be calculated by using Equation (3-6) (for readers' convenience, it is rewritten as Equation (8-2)).

$$g = \frac{52.80}{\left(\mu_{sv} + l_{loop}\right) \cdot \beta} \tag{8-2}$$

where l_{loop} is the loop detector length, μ_{SV} is the mean of the SV lengths, and β is the sensitivity correction parameter. A simple method for calibrating β is described in Section 3.2.2. By using intervals without LVs, the calculated constant *g* value can be applied to Equation (8-1) for speed estimates.

Section 3.2 described a revised region growing approach for separating intervals with LVs from those without. The algorithm was based on two assumptions: (1) there is at least one interval in a period that does not contain LVs, and (2) vehicle speeds are constant over the period. The algorithm works well when both assumptions hold. When traffic is congested or when LV volume is high, however, violating one or both assumptions, the revised region growing algorithm may result in biased speed estimates.

In order to identify SV-only intervals for speed estimates, video and single-loop sensors may be paired up at locations where both sensors exist. A paired video and single-loop (Paired VL) sensor system takes advantage of both video data and single-loop data. Because of the relative size differences between SVs and LVs, LVs can be easily identified from video data. However, because of the projection effect from a 3-dimentional space to a 2-dimentional plane, lane occupancy estimates from video data may contain remarkable errors, especially for video data captured by uncalibrated surveillance video cameras. Conversely, single-loop detectors provide accurate lane occupancy measurements but do not directly generate vehicle composition data.

Combining video data with single-loop data, therefore, may result in improved speed estimates.

8.2 ALGORITHM DESIGN

In the Paired VL sensor system, the VVDC system processes video data for interval LV volume estimates. Intervals containing LVs are discarded from the speed calculations. Therefore, intervals used for calculating speed estimates with Equation (8-1) are those containing only SVs. Because SV lengths vary narrowly around their mean, a constant *g* value calculated with Equation (8-2) can produce reasonably accurate speed estimates.

Video and single-loop sensors that form a Paired VL sensor system must be spatially close to each other. Ideally the single-loop detector should be visible in the video camera's field of view. Before the paired video and single-loop sensor data can be fused, the two data sequences must be time synchronized. The Paired VL sensor algorithm, therefore, contains three steps: (1) time and location synchronization between the selected single-loop sensor and the VVDC system, (2) LV interval identification, and (3) interval speed calculation. If an interval is identified as containing at least one LV, its measurements are not used for the speed calculation. Instead, the speed calculated from the previous interval is used as the speed for the current interval. Figure 8-1 shows the flow chart for this algorithm.

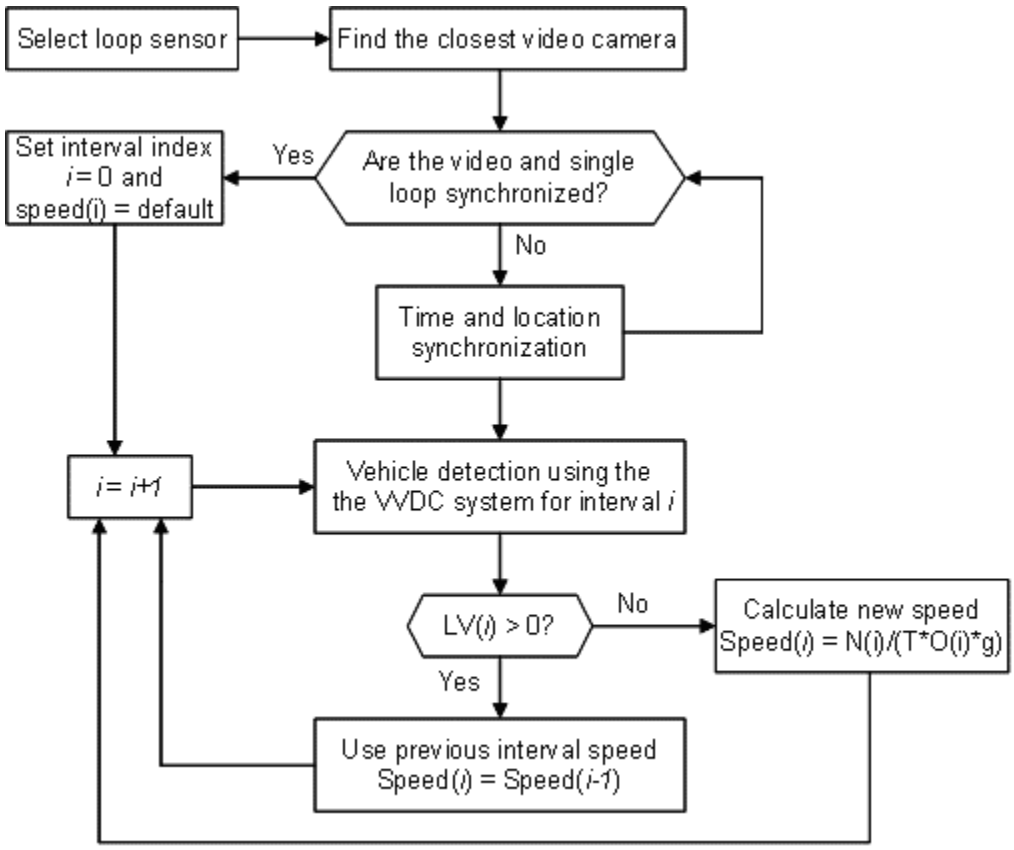

Figure 8-1: Flow Chart for the Paired VL Sensor Algorithm

8.2.1 Time Synchronization

It is very challenging to synchronize the clocks between the video and the single-loop data sequences because of uncertainties with the data collection, compression, and transmission processes. The video signal from a WSDOT surveillance camera is transmitted to a control cabinet via coaxial cable and then sent to a communications hub via fiber optic cable. At the communications hub, it is combined with video signals from many other cameras through the Frequency Division Multiplexing (FDM) technique. The combined video signals are then transmitted to the WSDOT TSMC in Shoreline via glass fiber. At the TSMC, the received video signals are de-multiplexed and connected

through a switch to a Digital VAX computer. This entire procedure is illustrated in Figure 8-2 (WSDOT, 2006).

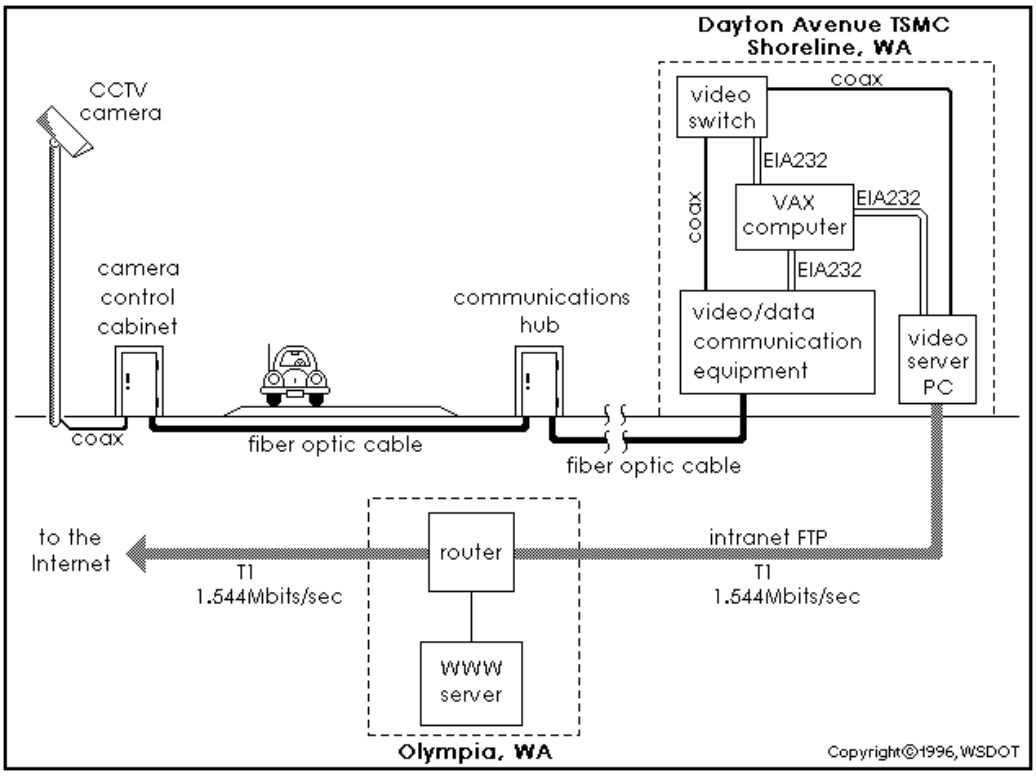

Figure 8-2: Schematic of the WSDOT Video Signal Communication System
Source: WSDOT (2006).

Video signals from the selected camera can be transmitted via live video feed fiber cable from the TSMC to the STAR Lab (details of this cable are discussed in Section 6.1). The latency of video signals received at the STAR Lab is approximately 30 milliseconds.

While the latency of the video data is relatively stable, the delay of loop detector data is volatile. A dual-loop's measurements are processed and integrated into 20-second intervals by the controller to which the dual-loop is connected. The calculated interval mean speed, vehicle length, and bin volume data are then shipped to the TSMC over the

WSDOT sensor data communication network. Depending on the level of congestion over the communications network, transmission delay varies. In addition to the transmission delay, system delay induced by the controller makes predicting total delay of the loop detector data more challenging. System delay is defined as the difference between the measurement time of a 20-second interval and the shipment time of the data to the TSMC. Although the controller clock is synchronized four times a day, the system delay for a particular loop cannot be easily estimated. At each WSDOT dual-loop station, the controller has a predefined order for stepping through the detector pairs. However, such an order is station dependent and cannot be identified by looking at the detector list. Controllers at dual-loop stations are configured for 40 detectors, but usually only 10 to 20 of them are defined. Suppose a dual-loop station has 20 inputs. The controller processes the detector pairs in the decreasing order of their input positions. For example, if a measurement data set was sent to the TSMC at 9:12:40, then the measurement interval for the dual loop connected to the first input position is 9:12:21 – 9:12:40 and that for the dual loop connected to the twentieth input position is 9:12:01 – 9:12:20. The system delay for each input position is shown in Table 8-1.

Table 8-1: Processing Delay for Each Input Position

Input Position	1	2	3	4	5	6	7	8	9	10	11	12	13	14	15	16	17	18	19	20
Delay (Seconds)	1	2	3	4	5	6	7	8	9	10	11	12	13	14	15	16	17	18	19	20

Because a detector may be attached to any input position, the mapping relationships between detector pairs and input positions at a dual-loop station are random.

We cannot determine the system delay for a given dual-loop detector from its location on the road.

As soon as interval measurements arrive at the TSMC server computer, they are time-stamped and broadcast by the loop_client application (see Section 3.3 for a brief description of loop_client) over the Internet. Because the time stamp of a data set includes both system delay and transmission delay, time synchronization of video and single-loop sensors becomes a very challenging issue. Time synchronization cannot be achieved by simply coordinating video and single-loop time stamps.

Although random delays are associated with the video or loop data transmission processes, these random delays account for a very small portion of overall delay. Therefore, the major portion of the time lag between video and single-loop time-stamps is relatively stable and can be identified through matching single-loop measured volumes and VVDC recorded volumes. Assume that this time lag is tl and $tl \in [tl_{min}, tl_{max}]$. Then the purpose of the synchronization process is to determine the value of tl. In this study, we propose a minimum-error-based approach for time synchronization. Because single-loop measurements are aggregated data of 20-second intervals, outputs from the VVDC system must be integrated into 20-second intervals for comparison. The VVDC system summarizes traffic counts into 20-second interval counts. The beginning time of each interval rotates from tl_{min} to tl_{max} with an increment of 1 second. This implies that each interval volume measured by a single-loop detector will have $vn = tl_{max} - tl_{min} + 1$ video measured volumes to compare to. After tm minutes, a total of 3*tm single-loop measured interval volumes are produced. Correspondingly, vn sets of interval volumes (each set contains 3*tm measurements) are produced by the VVDC system during the same period.

Equation (8-3) is then used to calculate the mean absolute errors between a video-measured volume sequence and the loop-measured volume sequence.

$$e_j = \frac{\sum_{i=1}^{3*tm} \left| V_L(t_i) - V_V(t_i + tl_{\min} + (j-1)*(tl_{\max} - tl_{\min})/(vn-1)) \right|}{3*tm} \tag{8-3}$$

where, e is the sum of absolute errors, j is video data sequence index, V_L is the loop measured interval volume, V_V is the VVDC system-produced interval volume, and t_i represents the ending time of interval $[t_i - 20, t_i]$. If

$$e_u \le e_j \quad \text{and} \quad e_u \le e_0 \qquad for\ j \in [1, vn] \tag{8-4}$$

then the u^{th} video sequence matches the single-loop volume sequence the best and is an acceptable match sequence based on the error threshold e_0. The time lag can be determined as

$$tl = t_{l\min} + (u-1)*(t_{l\max} - t_{l\min})/(vn-1) \tag{8-5}$$

Once *tl* is available, data from a paired video single-loop and video sensors can be fused for improved speed estimates.

8.2.2 LV Interval Identification

The VVDC system logs each detected vehicle with detection time and vehicle category information. When vehicles detected over a 20-second interval are counted for comparison, the VVDC system also checks to see whether one or more LVs are detected. Intervals containing at least one LV are marked as LV intervals. Data from LV intervals are not used to calculate speed.

8.2.3 Interval Speed Calculation

If an interval contains SVs only, its average vehicle length should be very close to the observed mean of the SV length distribution. This indicates that its *g* value can be approximated by using Equation (8-2). Given that SV lengths vary narrowly, the uniform vehicle length assumption required by Athol's equation can be satisfied. This ensures reasonably accurate speed estimates with Equation (8-1) for SV-only intervals.

For intervals with one or more LVs, average vehicle length may vary significantly from interval to interval. For these intervals, a constant *g* value is inappropriate for speed estimation with Equation (8-1). Because vehicle length is not available from single-loop measurements, calculating the *g* value for each interval is not realistic. However, because we do know the average length of SVs, and their length distribution has a narrow variance, we can calculate the speed for intervals that contain only SVs. Assuming that speeds do not vary much from interval to interval, we can use the speeds calculated for the SV-only intervals for other intervals that are adjacent or relatively close in time. Therefore, to avoid biased speed estimation, we drop intervals with LVs from the speed calculation. If an interval contains one or more LVs, the speed estimated for its nearest previous interval is assigned to the current interval.

9.0 SYSTEM DEVELOPMENT FOR PAIRED VIDEO AND SINGLE-LOOP SENSORS

9.1 SYSTEM DESIGN

A Paired VL system that implements the algorithm described in Section 8.2 was developed with Microsoft Visual C#. Figure 9-1 shows the flow chart for this system.

This Paired VL system is based on the ST-Estimator and the VVDC system introduced in Part II and Part III of this report. Live video feed is directly connected to system. A single-loop detector that matches the video location is manually specified by a user. Then the system can estimate speeds by fusing video and single-loop sensor data. As shown in Figure 9-1, the Paired VL system consists of four modules: the Vehicle Detection and Length Classification module, the Single-Loop Data Downloading module, the Time Synchronization module, and the Speed Estimation module. Details of each module are described in the section below.

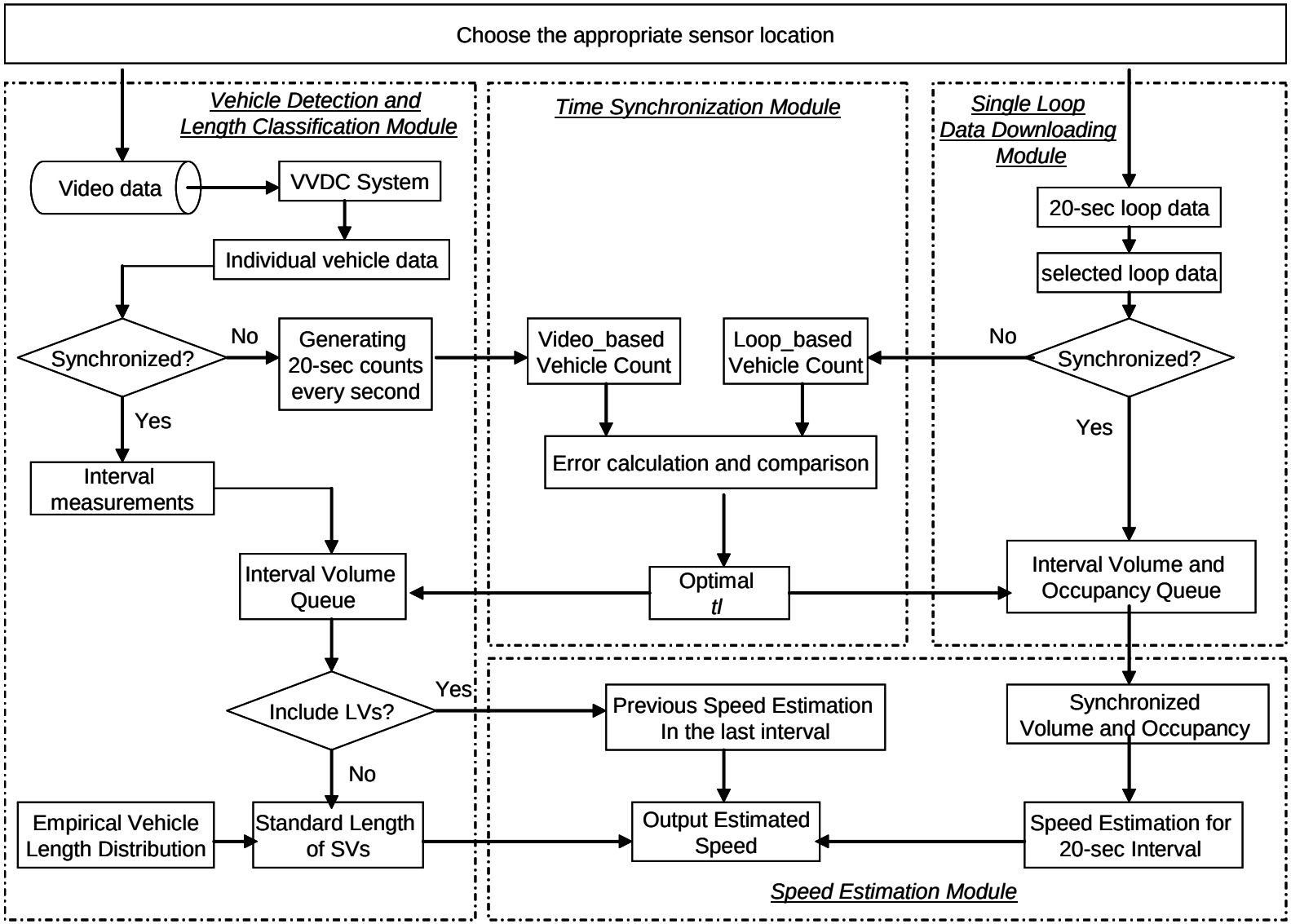

Figure 9-1: Flow Chart for the Paired VL System

9.2 SYSTEM IMPLEMENTATION

9.2.1 Vehicle Detection and Length Classification (VDLC) Module

The core of this module is the VVDC system. It takes live video input or digitized video images for vehicle counts and classification. The arrival time and type for each detected vehicle are logged by this module. If the video and single-loop data clocks have not been synchronized, the VDLC module integrates individual vehicle data from the video feed into 20-second interval counts every second. For example, it counts the number of vehicles detected from 9:30:20 through 9:30:39 at 9:30:40 and that from 9:30:21 through 9:30:40 at 9:30:41. After the system has been synchronized, this module produces a video-counted interval volume every 20 seconds. Also, a flag indicating whether this interval contains LVs is attached to the output of each interval. Readers are referred to Part III of this report for technical details on how the video-based vehicle detection and classification tasks are performed in the VVDC system.

9.2.2 Single-Loop Data Downloading (SLDD) Module

The function of the SLDD module is to secure single-loop data input. It uses the service provided by loop_client, an application developed by the UW ITS Research Program. The loop_client application broadcasts loop detector measurements every 20 seconds on a designated server port (by default, it uses 9004). The SLDD module connects to the loop_client server port with the TCP protocol to download all the loop detector data. The user then selects a particular loop and extracts data from the specified loop detector. If the clocks of the video and single-loop data have not been synchronized, the loop's 20-second interval measurements are sent to the Time Synchronization module

for time synchronization. Otherwise, loop data enter a data queue for the Speed Estimation module to use for speed estimates.

9.2.3 Time Synchronization (TS) Module

The TS module is a very important part of the Paired VL system because the video and single-loop data sequences cannot be properly fused without time synchronization. As metioned in Section 8.2.1, the time difference between the two clocks is affected by both transmission delay and system delay. However, direct measurement of transmission delay and system delay is very difficult to accomplish. Although individual vehicle arrival data are desirable for time synchronization, and the VVDC system is able to provide such data, we are not able to use such disaggregated data for time synchronization because the corresponding loop detector data to be synchronized with the VVDC data have been aggregated into 20-second intervals by the WSDOT loop detection system. Therefore, both video and loop clocks must be synchronized on the basis of 20-second vehicle counts. Each single-loop detected interval volume has *vn* video-based interval volumes to compare for the best match. For any interval, there may be more than one match. However, if one looks at *tm* minutes of data, there are 3**tm* available intervals. The chance of having multiple matches for all 3**tm* intervals decreases quickly as *tm* increases. Therefore, if *tm* is large enough, time synchronization can be satisfactorily achieved by using 20-second interval counts. In our implementation, all of the parameters used in our time sychronization approach (tl_{min}, tl_{max}, *tm*, and e_0) can be specified by users. The default values for these parameters are tl_{min}=-60 seconds, tl_{max}=60 seconds, *tm*=5 minutes, and e_0=0.3 vehicle/interval. Figure 9-2 shows a snapshot of the time synchronization interface.

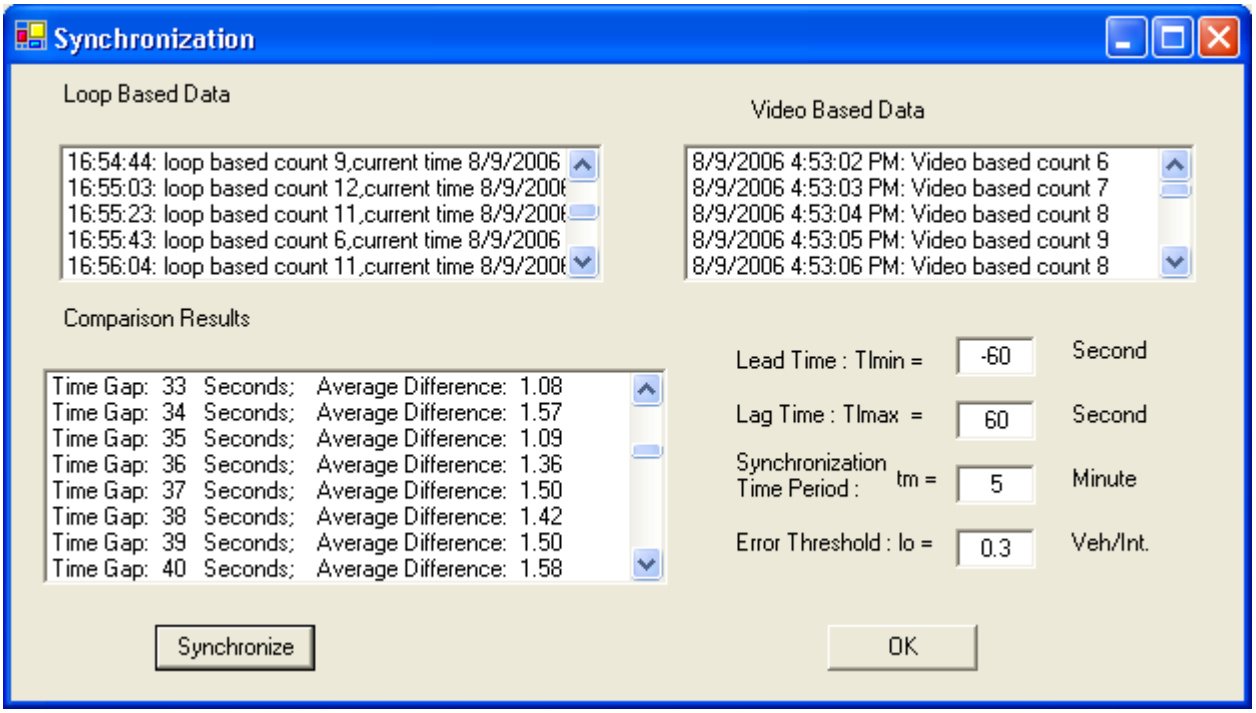

Figure 9-2: The Time Synchronization Module for Video and Loop Subsystems

The TS module calculates the sum of absolute error, e_j, by using Equation (8-3). Then it finds the *tl* that corresponds to the smallest sum of absolute error, e_u. Once the video and single-loop data time stamps have been synchronized, the Paired VL system recognizes the time difference between the video and single-loop data sequences. Proper adjustments are made to the data sequences so that they can be fused for improved speed estimates.

However, for cases in which the position of the single-loop detector is not visible in the video camera's field of view, time synchronization will be much more complicated because of the travel time variation between the virtual loop locations in the VVDC system and the actual single-loop locations. If vehicle speed varies significantly from

time to time, time synchronization may fail because no satisfactory *tl* can be found to satisfy Equation (8-4).

9.2.4 Speed Estimation (SE) Module

The SE module uses both the interval volume counted by the VVDC system and the interval volume and occupancy measured by the single-loop detectors for speed estimates. If the VVDC system has set the LV flag to true, then at least one LV is present in the current interval. Given the fact that the *g* value cannot be properly calculated when one or more LVs are present, the SE module does not conduct a speed calculation in this situation. Instead, it loads the most recent speed estimate as the current interval speed. If no LV is detected in the current interval, then, because of the features of SV length distribution, the *g* value calculated by Equation (8-2) should be very close to the ground truth *g* value. By using this *g* value, the space-mean speed for the current interval can be calculated with Equation (8-1). By pairing video and single-loop sensors, we can take advantage of the simplicity of Athol's algorithm and still avoid the speed estimation bias that would be introduced by intervals containing LVs. Figure 9-3 shows a snapshot of the speed estimation interface for the Paired VL system.

Given that the specific parameters used for speed estimation may be different from location to location, the SE module offers users a function for specifying the values for these parameters, such as the mean vehicle length and loop sensitivity correction coefficient. The SE module also plots the histogram of vehicle lengths for visual verification purposes. Additionally, the SE module provides users the freedom to use archived loop data. This function is especially useful for system tests in which recorded

videotapes and archived loop detector data may be used to evaluate system performance. Estimated speeds can be displayed on screen or stored in a user-specified output file.

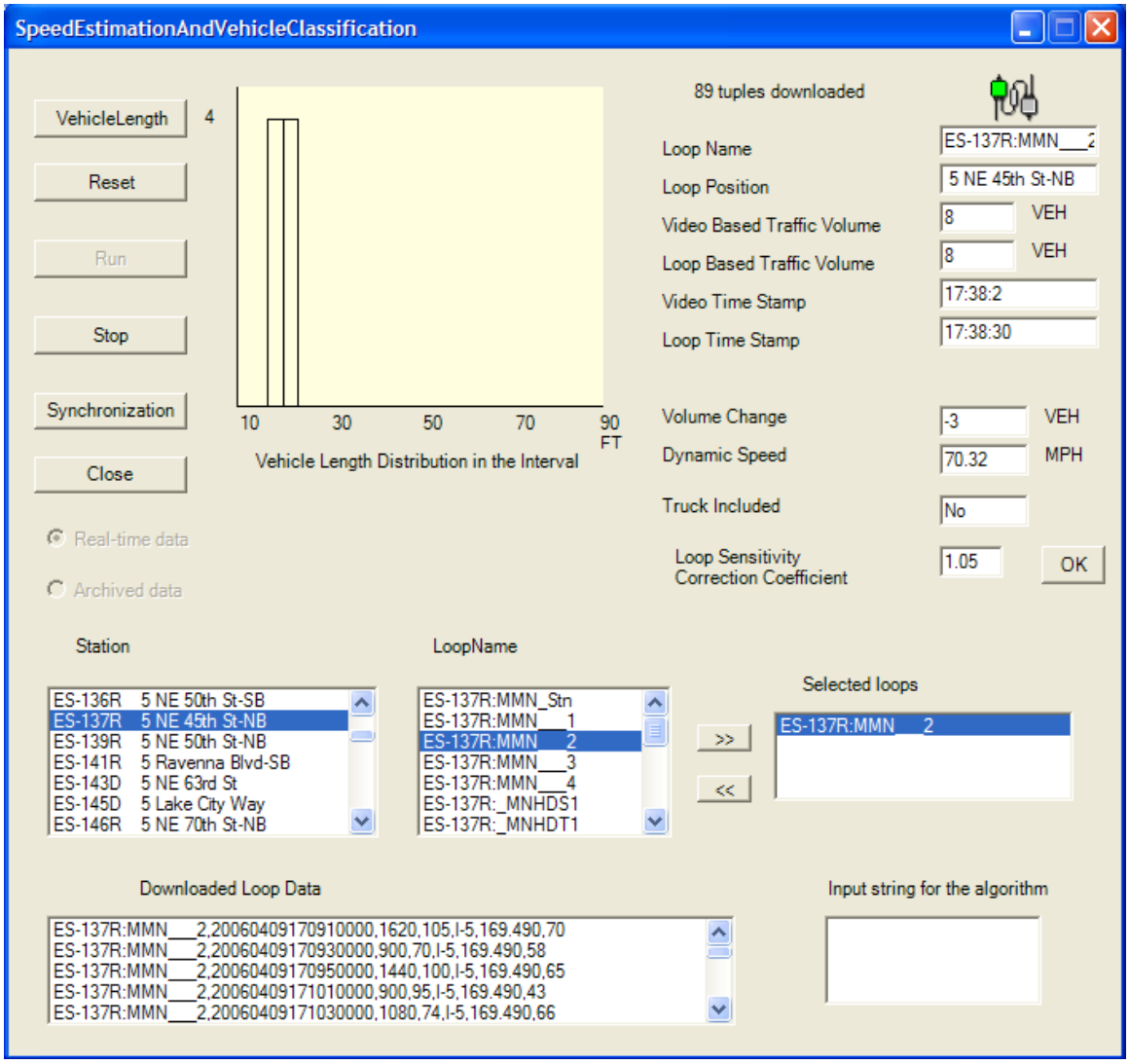

Figure 9-3: A Snapshot of Speed Estimation for a 20-Second Interval

10.0 TEST OF THE PAIRED VIDEO AND SINGLE-LOOP SYSTEM

10.1 TEST SITES AND DATA

Test sites must be selected on the basis of the following three criteria:

1. the paired video and single-loop sensors must be physically close to each other
2. the single-loop detectors must be part of dual-loop detector stations that are available and in good working condition
3. longitudinal occlusion is rare so that the VVDC system can produce reasonably accurate results.

With the help of WSDOT operational experts, two test sites were selected on northbound I-5 for testing the Paired VL system. Test site I comprised loop station ES-137R at milepost 169.79 on I-5 and the WSDOT surveillance video camera (ID = 12) at milepost 169.39 on I-5 near NE 45th Street. Test site II comprised loop station ES-168R at milepost 174.58 on I-5 and the WSDOT surveillance video camera (ID = 4) at NE 145th Street. The distance between the loop station and the camera was about 0.1 mile at this site.

For test site I, a virtual loop detector was placed on the second lane of northbound I-5 for video detection, as shown in Figure 10-1. Single-loop measurements from ES-137R: MMN__2 (the single loop on lane two) were fused with the data from this virtual loop. Similarly, a virtual loop and the single loop (ES-168R:MMN__2) on the second lane of northbound I-5 were paired on test site II. At both test sites, dual-loop detectors were available for speed and bin volume measurements. Dual-loop measured speeds were used to verify speeds estimated from the Paired VL system.

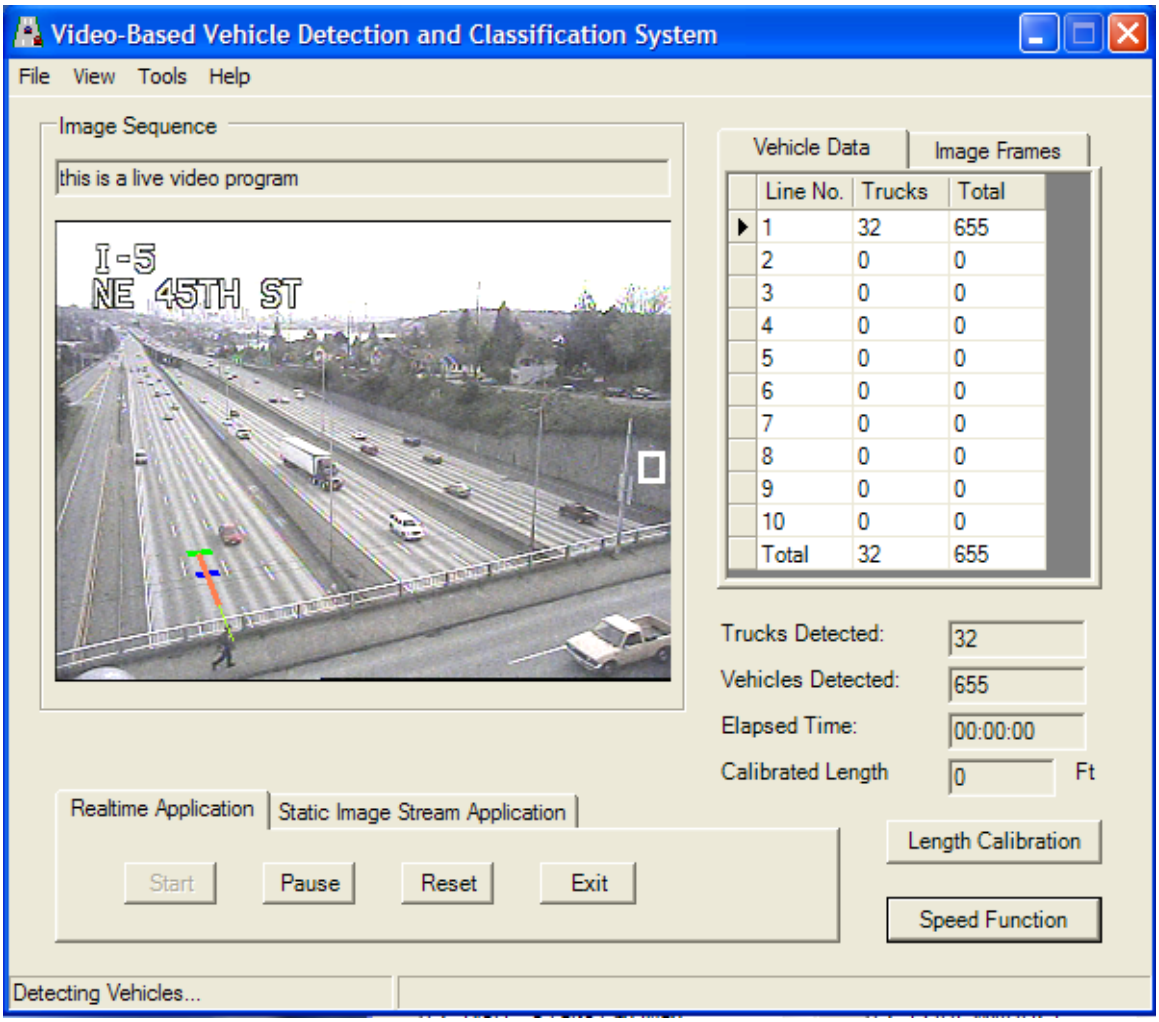

Figure 10-1: A Snapshot of Test Site I for the Paired VL System

10.2 TEST RESULTS AND DISCUSSION

The Paired VL system was tested for 60 minutes at each test site. To quantitatively evaluate the performance of the system, the authors defined a statistical variable called "estimation error." It was defined as the absolute difference between the estimated speed and the dual-loop observed speed for each 20-second interval. The Paired VL system was used to produce interval speed estimates. For comparison purposes, interval speeds were also estimated with the traditional algorithm, which directly applies unfiltered single-loop measurements to Equation (8-1) by using a

constant g value obtained from free-flow data for the site. The mean and standard deviation of estimation errors were calculated for each test case and for both the Paired VL and traditional algorithms. Table 10-1 shows the test results at both test sites, including dual-loop measured speeds, Paired VL system estimated speeds, traditional algorithm estimated speeds, and the estimation error statistics for each method.

Table 10-1: Online Test Results from the Two Test Locations

		Test Site One	Test Site Two
Loop Code & Camera ID		ES-137R:_MN__T2 & Camera ID 12	ES-168R:_MNN__2 & Camera ID 4
Location		NE 45th Street Northbound (milepost 169.39)	NE 145th Street Northbound (milepost 174.58)
Test Time Period		5:35-6:35 PM on 09-Apr-2006	11:00-12:00 PM on 12-Aug-2006
Loop Sensitivity Correction Coefficient		1.079	1.020
Mean of the Dual-Loop Observed Speeds		66.19	62.39
Mean of the Paired VL System Estimated Speeds		64.56	60.77
Mean of the Traditional Algorithm Estimated Speeds		64.47	60.23
Estimation Error for the Paired VL System (mph)	Mean	4.00	6.43
	Standard Deviation	4.30	5.81
Estimation Error for the Traditional Algorithm (mph)	Mean	4.41	7.01
	Standard Deviation	5.51	6.53

Before a test was started at each site, a 10-minute speed estimation was conducted to calibrate the loop sensitivity correction coefficient, β. The sensitivity correction coefficient was chosen so that the mean estimation error for the traditional algorithm was equal to zero. Then the same β was applied throughout the test period for both the Paired VL system and the traditional algorithm. For test site I, the mean and standard deviation of estimation error for the traditional algorithm were 4.41 mph and 5.51 mph,

respectively. Those for the Paired VL system were 4.00 mph and 4.30 mph, respectively. Obviously, the Paired VL system provided more accurate speed estimates. Speed curves for the dual-loop observed speeds, Paired VL system estimated speeds, and traditional algorithm estimated speeds are plotted in Figure 10-2.

For test site II, the estimation error statistics showed that the Paired VL system also performed better than the traditional algorithm. Figure 10-3 provides visual comparisons of the speed curves for test site II.

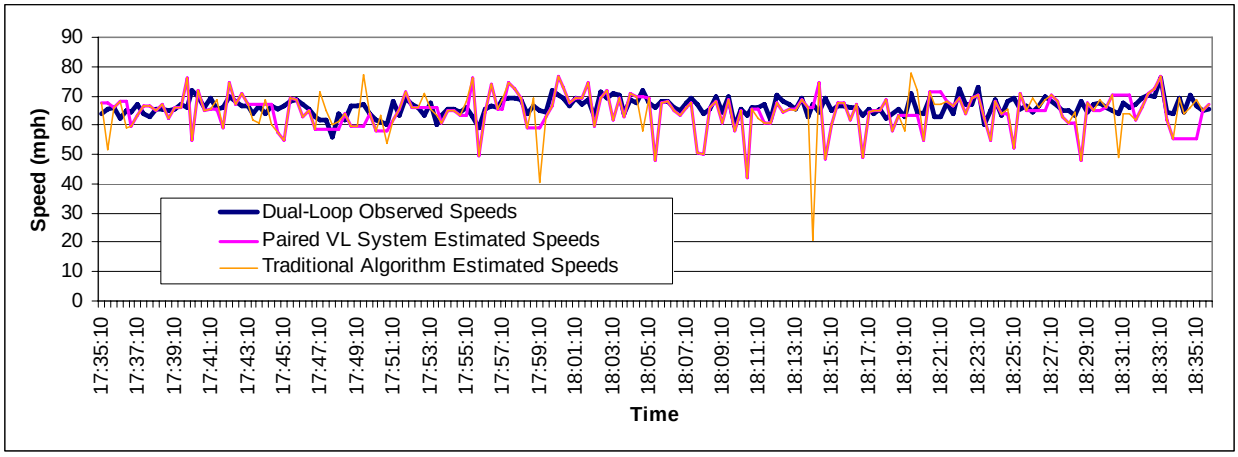

Figure 10-2: Comparison between Observed Speeds and Estimated Speeds at Test Site I

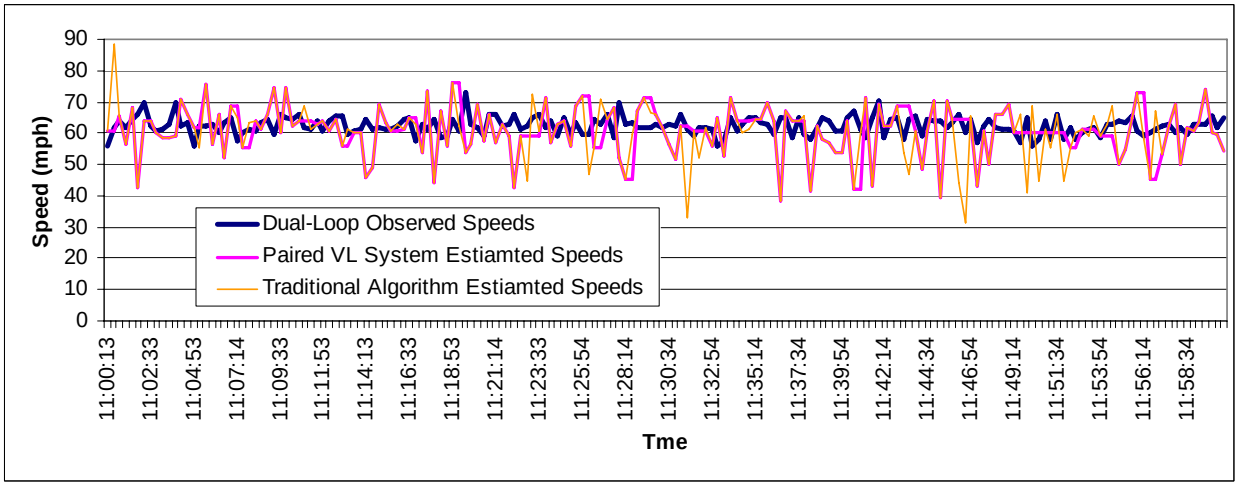

Figure 10-3: Comparison between Observed Speeds and Estimated Speeds at Test Site II

We can see that in both figures 10-2 and 10-3, the speed curves generated by the Paired VL system are closer to the dual-loop speed curves than the curves generated by the traditional algorithm. This shows that the Paired VL system provided better speed estimates than the traditional algorithm, which has been widely used by traffic systems management centers for traffic speed estimation.

During the test process, we noticed that false dismissals of long vehicles were a major source of mistakes generated by the Paired VL system. If an interval contains one or more LVs but is not flagged as an LV interval, the Paired VL system will provide biased speed estimates. Conversely, longitudinal occlusion may generate false alarms of LVs and hence make speed updates less frequent. In addition to the two major error causes, random delays during data transmission may disturb the synchronized process in fusing video and single-loop data and result in speed estimation errors.

Note that both tests were conducted under un-congested conditions. Because the current VVDC system is not capable of producing good vehicle detection and classification data under traffic conditions with significant vehicle occlusions, the authors were not able to test the Paired VL system under congested scenarios. Nonetheless, the concept of the paired video and single-loop sensor system was demonstrated to a certain extent.

10.3 TEST SUMMARY FOR THE PAIRED VL SYSTEM

To improve the accuracy of traffic speed estimation, a paired video and single-loop sensor algorithm was developed and implemented as the Paired VL system described in this report. The algorithm combines video-based vehicle detection and classification results with single-loop measurements to avoid the biased impacts of LVs

on traffic speed estimates. Two test sites were selected to evaluate the performance of the Paired VL system. The means of estimation error for the Paired VL system were 4.00 mph and 6.43 mph for test sites I and II, respectively. In comparison to the speed estimates produced by the traditional algorithm, the Paired VL system produced better speed estimation accuracy in both tests.

Investigation of Paired VL system errors showed that false dismissals of trucks and longitudinal occlusions were major causes of speed estimation errors. Also, random delays during data transmission could sometimes disturb the synchronized data sequences and result in estimation errors.

PART V SUMMARY

11.0 CONCLUSIONS AND RECOMMENDATIONS

11.1 CONCLUSIONS

Traffic speed and truck volume data are important variables for transportation planning, pavement design, traffic safety, traffic operations, and car emission control. However, these data are not directly measured by single-loop detectors, the most widely available type of sensor on the existing roadway network. To obtain quality estimates of traffic speed and truck volume data with existing freeway surveillance equipment, several algorithms were developed and implemented in this study.

First, a new speed estimation algorithm that uses single-loop data was developed. This algorithm implements the region growing mechanism commonly used in video image processing. This region growing algorithm, together with the vehicle classification algorithm developed by Wang and Nihan (2003), was implemented in the ST-Estimator for improved speed and truck volume data. In tests of the ST-Estimator, the new speed algorithm outperformed both the traditional algorithm and the speed estimation algorithm developed by Wang and Nihan (2003). By using the speed estimated with this algorithm, LV volumes were estimated with the approach based on the Nearest Neighbor Decision rule. LV volume errors estimated at three test locations (the second lanes at Station ES-167D, station ES-172R, and station ES-209D) were within 7.5 percent over a 24-hour period. The ST-Estimator test results indicated that the ST-Estimator can be applied to obtain reasonably accurate speed and LV volume estimates at single-loop stations.

Second, several computer-vision based algorithms were developed or applied to extract the background image from a video sequence, detect the presence of vehicles,

identify and remove shadows, and calculate pixel-based vehicle lengths for classification. These algorithms were implemented in the prototype VVDC system written with the Microsoft Visual C#. As a plug and play system, the VVDC system is capable of processing live video signals in real time. A WinTV-USB card was used to capture live video images. The VVDC system can also be used to process digitized video images in the JPEG or BMP formats. Because the VVDC system does not require camera calibration, it can be easily applied to locations with existing surveillance video cameras. Also, users are allowed to specify the bin length threshold to collect desired types of vehicles with the VVDC system.

The VVDC system was tested at three test locations under different traffic and environmental conditions. The accuracy of vehicle detection was over 97 percent, and the total truck count error was lower than 9 percent for all three tests. This implies that the video image processing method developed for vehicle detection and classification in this study is indeed a viable alternative for truck data collection. However, the prototype VVDC system is currently designed to work in daytime lighting and under conditions without longitudinal vehicle occlusion and severe camera vibration.

Third, a speed estimation algorithm using paired video and single-loop sensor inputs was designed. The core idea of this algorithm is to use a video sensor to screen out intervals containing LVs before using single-loop measurements for speed estimation. The traditional speed estimation algorithm is based on the assumption of uniform vehicle length. When a significant number of LVs are present in a traffic stream, the mean effective vehicle length may vary significantly from interval to interval and hence violate the uniform vehicle length assumption. If intervals containing LVs are used in the speed

calculations, biased speed estimates will result. The paired video and single-loop sensors rely on video image processing for LV detection and single-loop data for speed calculation. If an interval is identified as containing one or more LVs, its single-loop measurements are dropped from the speed calculations. Instead, the most recently calculated interval speed is assigned to the interval containing LVs. A paired video and single-loop algorithm was implemented in the Paired VL system described in this report. Video and single-loop data from two test sites were used to evaluate the performance of the Paired VL system. The authors' experiments indicated that speeds estimated by the Paired VL system were more accurate than speeds estimated by the traditional algorithm. Extreme values resulting from LV presence were effectively eliminated. However, finding a location with both video and single-loop sensors may not be easy. Also, time synchronization for the Paired VL system is very challenging, and detection errors from the video sensor may significantly degrade the performance of the Paired VL system. All these factors cast shadows over the applicability of the Paired VL system, although the potential effectiveness of the idea was demonstrated in this study.

In short, several algorithms and corresponding computer tools were developed for improved speed and truck data in this study. The authors conclude that quality speed and truck volume data can be estimated from single-loop data by applying the ST-Estimator. Although the prototype VVDC system now works only under certain restricted conditions, the potential utility and effectiveness of the system were demonstrated, and the authors conclude that further development of the VVDC system is warranted. Given that surveillance video cameras have been increasingly deployed in recent years, the VVDC system can be a cost-effective solution for turning such surveillance video

cameras into video detectors when necessary. For locations with both video and single-loop sensors, speed estimates can be improved by combining video data with single-loop data.

11.2 RECOMMENDATIONS

The authors recommend further studies in the following two directions:

(1) Improve the accuracy and applicability of the VVDC system. Major issues deserving further research effort include the following:

- Traffic occlusion. Traffic occlusion typically results from inappropriate video camera location, flat pitch angle of cameras, and heavy traffic volumes on the road. Some mathematic models, such as the Markov Random Field models and motion-based features, may be used to handle this problem.
- Camera vibration. Most surveillance video cameras have vibration problems due to wind or road infrastructure shaking. Algorithms based on background subtraction are extremely sensitive to camera vibrations. Feature-based detection may be a good solution to this problem.
- Reflection. In front fire detection, reflection of vehicle headlights may cause early detection and overestimation of vehicle length. Models for reflection rejection are needed to improve the accuracy of the VVDC system.

(2) Investigation of loop detector data accuracy. When the Paired VL system was tested, the authors found that video-recorded, 20-second counts sometimes varied significantly from single-loop counts. This vehicle count inconsistency made it very difficult to synchronize the video and single-loop clocks. In the process of finding good test sites, the authors studied loop data quality at several stations by comparing the

ground-truth volumes resulting from manual video counts with single-loop measured volumes. The authors found that many single-loop detectors have noticeable problems of false alarms and false dismissals. The Paired VL system could be easily modified to be an effective tool for verifying the working status of loop detectors.

The authors believe that an improved VVDC system would be very useful for collecting freeway speed and truck volume data. It could also be applied to collect intersection performance measures by using onsite surveillance or detection cameras. In addition to the computer that hosts the VVDC system, a WinTV card is the only piece of hardware required. The VVDC system, therefore, could provide a cost-effective solution for automatic traffic data collection at locations with surveillance or detection cameras.

ACKNOWLEDGMENTS

The authors would like to acknowledge the financial support for this project from Transportation Northwest (TransNow), the USDOT University Transportation Center for Federal Region 10, and the Washington State Department of Transportation. The authors also wish to express sincere appreciation to WSDOT and TransNow personnel, specifically Morgan Balogh, Pete Briglia, Vinh Dang, Mark Morse, Michael Forbis, John Rosen, and David Bushnell, for their valuable suggestions and kind help in setting up the video-feed link to the STAR Lab. Special thanks to Dr. Dan Dailey and Mr. Fritz Cathey for providing and trouble shooting the video switch program.

REFERENCES

American Association of State Highway and Transportation Officials (AASHTO). 2004. *A Policy on Geometric Design of Highways and Streets*. Fifth Edition, AASHTO, Washington D.C.

Anderson, I.B. and R.A. Krammes. 2000. New Consistency Model for Rural Highways and Its Relationship to Safety. *ASCE Journal of Transportation Engineering*, Vol. 130, No. 3. 286-293.

Aredonk, J. 1996. A comparison of real-time freeway speed estimation using loop detectors and AVI technologies. *Compendium: Graduate Student Papers on Advanced Surface Transportation Systems*, Southwest Region University Transportation Center, Texas Transportation Institute, Texas A&M University System, College Station, TX, J-i – J-140.

Avery, R. P., Y. Wang and G. S. Rutherford. 2004. Length-Based Vehicle Classification Using Images from Uncalibrated Video Cameras. Proceedings of the *7th International IEEE Conference on Intelligent Transportation Systems*, pp. 737-742.

Athol, P. 1965. Interdependence of Certain Operational Characteristics within a Moving Traffic Stream. *Highway Research Record 72*, pp. 58-87.

Bonneson, J. and M. Abbas. 2002. *Video Detection for Intersection and Interchange Control*. FHWA/TX-03/4285-1. Texas Transportation Institute. College Station, Texas.

Canny, J. 1986. A Computational Approach to Edge Detection. *IEEE Transactions on Pattern Analysis and Machine Intelligence*, Vol. 8, No. 6, pp. 679-698.

Cheevarunothai, P., Y. Yang and N. L. Nihan. 2005. Development of Advanced Loop Event Data Analyzer (ALEDA) for Investigations of Dual-Loop Detector

Malfunctions. *Proceeding CD-Rom for the 12th World Congress on Intelligent Transportation Systems*, San Francisco, California.

Cherrett, T., H. Bell, M. McDonald. 2000. Traffic Management Parameters from Single Inductive Loop Detectors. Transportation Research Record, No. 1719, 112-120, Washington D.C.

Coifman, B. 2001. Improved Velocity Estimation Using Single Loop Detectors. *Transportation Research, Part A,* Vol. 35, No. 10, 863-880.

Coifman, B., S. Dhoorjaty, and Z. Lee. 2003. Estimating Median Velocity Instead of Mean Velocity at Single Loop Detectors. *Transportation Research, Part C,* Vol. 11, No. 3-4, 211-222.

Courage, K. G., C. S. Bauer, and D. W. Ross. 1976. Operating parameters for main-line sensors in freeway surveillance systems, *Transportation Research Record 601*, TRB, National Research Council, Washington, D.C., pp. 19-26.

Cucchiara, R., C. Grana, M. Piccardi, and A. Prati. 2003. Detecting Moving Objects, Ghosts, and Shadows in Video Streams. *IEEE Transactions on Pattern Analysis and Machine Intelligence*, Vol. 25, No. 10, pp. 1337-1342.

Cunagin, W.D. and C.J. Messer. 1983. Passenger Car Equivalents for Rural Highways. *Transportation Research Record 905*, TRB, National Research Council, Washington, D.C., pp. 61-68.

Dailey, D.J. 1999. A Statistical Algorithm for Estimating Speed from Single Loop Volume and Occupancy Measurements. *Transportation Research B*, Vol. 33B, No. 5, pp. 313-22

EPA (US Environmental Protection Agency). 2001. *National Air Quality and Emissions Trends Report, 1999*. EPA 454/R-01-004. EPA. North Carolina.

Fung, G.S.K., N.H.C. Yung, G.K.H. Pang, and A.H.S. Lai. 2002. Effective Moving Cast Shadow Detection for Monocular Color Traffic Image Sequences. *Optical Engineering*, Vol. 41, No. 6, pp. 1425-1440.

Gamba, P., M. Lilla, and A. Mecocci. 1997. A Fast Algorithm for Target Shadow Removal in Monocular Colour Sequences. Proceedings of the *International Conference on Image Processing*, Vol. 1, pp. 436-447.

Gerlough, D. L., and M. J. Huber. 1975. *Traffic Flow Theory, A Monograph,* TRB Special Report 165, TRB, National Research Council, Washington, D.C.

Graettinger, A.J., R.R. Kilim, M.R. Govindu, P.W. Johnson, and S.R. Durrans. 2005. Federal Highway Administration Vehicle Classification from Video Data and a Disaggregation Model. *Journal of Transportation Engineering*, Vol. 131, No. 9. pp. 689-698.

Gronbeck, C. 2004. *SunAngle*. Accessed online at http://www.susdesign.com/sunangle/ on 09 December 2005.

Gu, X., D. Yu, and L. Zhang. 2005. Image Shadow Removal Using Pulse Coupled Neural Network. *IEEE Transactions on Neural Networks*, Vol. 16, Issue 3, pp. 692-698.

Gupte, S., O. Masoud, R.F.K. Martin, and N.P. Papanikolopoulos. 2002. Detection and Classification of Vehicles. *IEEE Transactions on Intelligent Transportation Systems*, Vol. 3, No. 1, pp. 37-47.

Hallenbeck, M. 1993. Seasonal Truck Volume Patterns in Washington State. *Transportation Research Record 1397*, TRB, National Research Council, Washington, D.C., pp. 63-67.

Hasegawa, O. and T. Kanade. 2005. Type Classification, Color Estimation, and Specific Target Detection of Moving Targets on Public Streets. *Machine Vision and Applications*, Vol. 16, No. 2, pp. 116-121.

Hellinga, B. R. 2002. Improving Freeway Speed Estimates from Single-Loop Detectors. *ASCE Journal of Transportation Engineering*, 128(1), 58-67.

Hsieh, C., E. Lai, Y. Wu, and C. Liang. 2004. Robust, Real Time People Tracking with Shadow Removal in Open Environment. *5th Asian Control Conference*, Vol. 2, pp. 901-905.

ITE (Institute of Transportation Engineers). 1997. *Traffic Detector Handbook*. Second Edition. ITE. Washington D.C.

Kim, J.J., S. Smorodinsky, M. Lipsett, B.C. Singer, A.T. Hodgson, and B. Ostro. 2004. Traffic-related Air Pollution near Busy Roads: The East Bay Children's Respiratory Health Study. *American Journal of Respiratory and Critical Care Medicine*, Vol. 170, pp. 520-526.

Kwon, J., P. Varaiya, and A. Skabardonis. 2003. Estimation of Truck Traffic Volume from Single Loop Detector Using Lane-to-Lane Correlation. Preprint CD-ROM from the *82nd Annual Meeting of Transportation Research Board*.

Lai, A.H.S., G.S.K. Fung, and N.H.C. Yung. 2001. Vehicle Type Classification from Visual-Based Dimension Estimation. Proceedings of the *IEEE Intelligent Transportation Systems Conference*, Oakland, CA, pp. 201-206.

Lo, B.P.L., S. Thiemjarus, and G. Yang. 2003. Adaptive Bayesian Networks for Video Processing. Proceedings of the *2003 International Conference on Image Processing*, Vol. 1, pp. 889-892.

Martin, P.T., G. Dharmavaram, and A. Stevanovic. 2004. *Evaluation of UDOT's Video Detection Systems: System's Performance in Various Test Conditions*. Report No: UT-04.14. Salt Lake City, Utah.

Michalopoulos, P.G. 1991. Vehicle Detection Video Through Image Processing: The Autoscope System. *IEEE Transactions on Vehicular Technology*, Vol. 40, No. 1. pp. 21-29.

Microsoft Inc. 2002. Microsoft DirectX Web site. Accessed on Oct. 16, 2005 at http://www.microsoft.com/windows/directx/default.aspx.

Mikhalkin, B., H. J. Payne, and L. Isaksen. 1972. Estimation of speed from presence detectors, *Highway Research Record 388*, HRB, National Research Council, Washington, D.C., 1972, pp. 73-83.

National Highway Traffic Safety Administration (NHTSA). 2004. *Traffic Safety Facts 2003: A Compilation of Motor Vehicle Crash Data from the Fatality Analysis Reporting System and the General Estimates System*. US Department of Transportation, National Highway Traffic Safety Administration, Washington, D.C.

Otsu, N. 1979. A Threshold Selection Method from Gray-Level Histograms. *IEEE Transactions on Systems, Man and Cybernetics*, Vol. 9, No. 1, pp. 62-66.

Peters, A., S. von Klot, M. Heier, I. Trentinaglia, A. Hörmann, H.E. Wichmann, and H. Löwel. 2004. Exposure to Traffic and the Onset of Myocardial Infarction. *The New England Journal of Medicine*, Vol. 351, No. 17, pp. 1721-1730.

Petty, K.F., P. Bickel, M. Ostland, J. Rice, F. Schoenberg, J. Jiang, and Y. Ritov. 1998. Accurate Estimation of Travel Times from Single-Loop Detectors. *Transportation Research, Part A*, Vol. 32, No. 1, 1-17.

Prati, A., I. Mikic, M.M. Trivedi, and R. Cucchiara. 2003. Detecting Moving Shadows: Algorithms and Evaluation. *IEEE Transactions on Pattern Analysis and Machine Intelligence*, Vol. 25, No. 7, pp. 918-923.

Pushkar, A., F. L. Hall, and J.A. Acha-Daza. 1994. Estimation of speeds from single-loop freeway flow and occupancy data using cusp catastrophe theory model. *Transportation Research Record*, No. 1457, 149-157, Washington, D.C.

Rad, R. and M. Jamzad. 2005. Real Time Classification and Tracking of Multiple Vehicles in Highways. *Pattern Recognition Letters*, Vol. 26, No. 10, pp. 1597-1607.

Rhodes, A., D.M. Bullock, J. Sturdevant, Z. Clark, and D.G. Candey, Jr. 2005. Evaluation of Stop Bar Video Detection Accuracy at Signalized Intersections. Proceedings of the *84th Annual Meeting of Transportation Research Board* (CD-Rom), Washington D.C.

Scanlan, J.M., D.M. Chabries, and R.W. Christiansen. 1990. A Shadow Detection and Removal Algorithm for 2-D Images. Proceedings of the *International Conference on Acoustics, Speech, and Signal Processing*, Vol. 4, pp. 2057-2060.

Shapiro, L. G. and G. C. Stockman. 2001. *Computer Vision*. Prentice Hall, New Jersey, pp. 289-290.

Sun, C., and S.G. Ritchie. 1999. Individual Vehicle Speed Estimation Using Single Loop Inductive Waveforms. *Journal of Transportation Engineering,* Vol. 125, No. 6, 531 - 538.

Tian, Z.Z., M.D. Kyte, and C.J. Messer. 2002. Parallax Error in Video-Image Systems. *Journal of Transportation Engineering*, Vol. 128 (3), pp. 218-223.

Transportation Research Board (TRB). 2000. *Highway Capacity Manual*. TRB, National Research Council, Washington, D.C.

University of Washington Intelligent Transportation Systems (UW ITS) Research Program. 1997. loop_client: Real-Time Freeway Sensor Information Over The Internet. Accessed online at http://www.its.washington.edu/software/loop_cli.html.

Wang, J.M., Y.C. Chung, C.L. Chang, and S.W. Chen. 2004. Shadow Detection and Removal for Traffic Images. *IEEE International Conference on Networking, Sensing and Control*, Vol. 1, pp. 649-654.

Wang, Y., and N.L. Nihan. 2000. Freeway traffic speed estimation using single loop outputs, *Transportation Research Record*, No. 1727, 120-126, TRB, National Research Council, Washington, D.C.

Wang, Y. and N.L. Nihan. 2003. Can Single-Loop Detectors Do the Work of Dual-Loop Detectors? *ASCE Journal of Transportation Engineering*, 129(2), pp. 169-176.

Washington State Department of Transportation (WSDOT). 2002. *2001 Annual Traffic Report*, Seattle, Washington.

Washington State Department of Transportation (WSDOT). "Seattle Area Traffic Frequently Asked Questions." Website at http://www.wsdot.wa.gov/Traffic/seattle/questions/, Accessed Feb. 20, 2006.

Weber, A. N. 1999. *Verification of Radar Vehicle Detection Equipment Study SD98-15 Final Report*. South Dakota Department of Transportation, 1999.

Xu, L., J.L. Landabaso, and M. Pardas. 2005. Shadow Removal with Blob-Based Morphological Reconstruction for Error Correction. Proceedings of the *IEEE International Conference on Acoustics, Speech, and Signal Processing*, Vol. 2, pp. 729-732.

Zhang, X., Y. Wang, and N.L. Nihan. 2003. Investigating Dual-Loop Errors Using Video Ground-Truth Data. Proceedings of *the 13th Annual Meeting of ITS America (CD-Rom)*. Paper 158.

Zheng, J., Y. Wang, N.L. Nihan, and M.E. Hallenbeck. 2006. Extracting Roadway Background Image: a Mode-Based Approach. *Transportation Research Record*. In Press.